UC San Diego
UC San Diego Previously Published Works

Title

Zinc-finger PARP proteins ADP-ribosylate alphaviral proteins and are required for interferon-γ-mediated antiviral immunity.

Permalink

https://escholarship.org/uc/item/33g0k10d

Journal

Science Advances, 11(5)

Authors

Ryan, Andrew

Delgado-Rodriguez, Sofia

Daugherty, Matthew

Publication Date

2025-01-31

DOI

10.1126/sciadv.adm6812

Peer reviewed

VIROLOGY

Zinc-finger PARP proteins ADP-ribosylate alphaviral proteins and are required for interferon-γ–mediated antiviral immunity

Andrew P. Ryan, Sofia E. Delgado-Rodriguez, Matthew D. Daugherty*

Viral manipulation of posttranslational modifications (PTMs) is critical to enable control over host defenses. Evidence suggests that one such PTM, adenosine 5′-diphosphate (ADP)–ribosylation, is important for viral replication, but the host and viral components involved are poorly understood. Here, we demonstrate that several human poly(ADP-ribose) polymerase (PARP) proteins, including the zinc-finger domain containing PARP7 (TiPARP) and PARP12, directly ADP-ribosylate the alphaviral nonstructural proteins (nsPs), nsP3 and nsP4. These same human PARP proteins inhibit alphavirus replication in a manner that can be antagonized by the ADP-ribosylhydrolase activity of the virally encoded macrodomain. Last, we find that knockdown of any of the three CCCH zinc-finger domain containing PARPs, PARP7, PARP12, or the enzymatically inactive PARP13 (ZAP/ZC3HAV1), attenuates the antiviral effects of interferon-γ on alphavirus replication. Combined with evolutionary analyses, these data suggest that zinc-finger PARPs share an ancestral antiviral function that can be antagonized by the activity of viral macrodomains, indicative of an ongoing evolutionary conflict between host ADP-ribosylation and viruses.

INTRODUCTION

Adenosine 5′-diphosphate (ADP)–ribosylation is a ubiquitous and reversible posttranslational modification of proteins that is found in all domains of life (1–5). The cycle of ADP-ribosylation begins with the enzymatic addition (i.e., "writing") of ADP-ribose (ADPr) to a target protein by a variety of ADP-ribosyltransferases using the metabolic cofactor NAD$^+$ (nicotinamide adenine dinucleotide) as the substrate (2–5). In addition to the wide range of target amino acids that can be modified, ADPr can also be added in either a monomeric form [mono-ADP-ribosylation (MARylation)] or large, branching or linear chains of variable size and structure [poly-ADP-ribosylation (PARylation)] (1–5). Recognition (i.e., "reading") of ADP-ribosylation can be accomplished by diverse protein domains, including macrodomains and WWE, BRCT, and PBZ domains, while the removal of ADPr (i.e., "erasing") can be catalyzed by several distinct protein domains, including macrodomains, ARH domains, and Nudix hydrolase domains (1, 5, 6).

In humans, intracellular ADP-ribosylation is catalyzed by members of the 17-member PARP protein family (4). While the most well-studied poly(ADP-ribose) polymerase (PARP), PARP1, resides in the nucleus and catalyzes poly-ADP-ribosylation, most human PARPs are cytoplasmically localized and catalyze MARylation (3, 4, 7). In addition to the PARP domain, human PARPs contain a breadth of associated protein domains and architectures, including RNA-binding zinc-finger domains, and ADPr-binding domains including WWE domains and macrodomains (3, 4, 7) (Fig. 1A). Notably, the protein targets and functional roles of many PARPs, especially the cytoplasmic MARylating enzymes, are poorly understood.

One emerging area of ADP-ribosylation function is in antiviral immunity and regulation of viral replication (8–12). Several human PARP genes are up-regulated during viral infection or upon cellular treatment with immune signaling cytokines including type I interferon [interferon-α (IFN-α) and IFN-β] and type II interferon (IFN-γ)

Department of Molecular Biology, School of Biological Sciences, University of California, San Diego, La Jolla, CA 92093, USA.
*Corresponding author. Email: mddaugherty@ucsd.edu

(8–10, 12). Likewise, numerous PARPs have been shown to either regulate antiviral signaling or directly repress viral replication, including PARP7 (TiPARP), PARP9, PARP10, PARP12, PARP13 (zinc-finger antiviral protein (ZAP) or ZC3HAV1), and PARP14 (8–14), although the importance of ADP-ribosylation in many of these processes has not been determined. Consistent with the role of host PARPs in antiviral immunity, nearly one-third of human PARPs also display strong signatures of rapid evolution that are characteristic of genes engaged in evolutionary "arms races" with viruses (15, 16). Perhaps the most compelling argument for ADP-ribosylation being critical in the conflict between host immunity and viral replication is the presence of macrodomains in several families of important human viral pathogens, including Togaviridae [e.g., Semliki Forest virus (SFV) and chikungunya virus], Coronaviridae [e.g., SARS-CoV-2 (severe acute respiratory syndrome coronavirus 2)], and Hepeviridae (e.g., hepatitis E virus) (8–11, 17, 18). In many cases, the ability of the macrodomain to bind ("read") or remove ("erase") ADP-ribosylation is critical to the replication success or pathogenesis of these viruses (12, 19–26), although the exact mechanisms behind these macrodomain-mediated processes are not fully elucidated.

Given the preponderance of evolutionary, genetic, and functional evidence for a host-virus conflict surrounding ADP-ribosylation, we set out in this work to test whether any specific host PARPs directly ADP-ribosylate alphavirus proteins, whether alphaviral macrodomains can remove such ADP-ribosylation, and what effects perturbation of host PARPs and viral macrodomains have on viral replication. Here, we reveal that the CCCH zinc-finger PARPs, PARP7 and PARP12, as well as the macrodomain-containing PARP15, can ADP-ribosylate one or more nsPs from two alphaviruses, SFV and Sindbis virus (SinV). We also find that alphaviral macrodomains can effectively reverse the ADP-ribosylation catalyzed by PARP12 and PARP15 and, to a lesser degree, PARP7. Consistent with alphaviral macrodomains directly antagonizing the antiviral activity of host PARP-mediated ADP-ribosylation, we find that overexpression of viral ADP-ribosylating PARPs (PARP7, PARP12, and PARP15) strongly inhibit an SFV replication reporter that lacks macrodomain activity, but this PARP-mediated antiviral effect is repressed when the viral
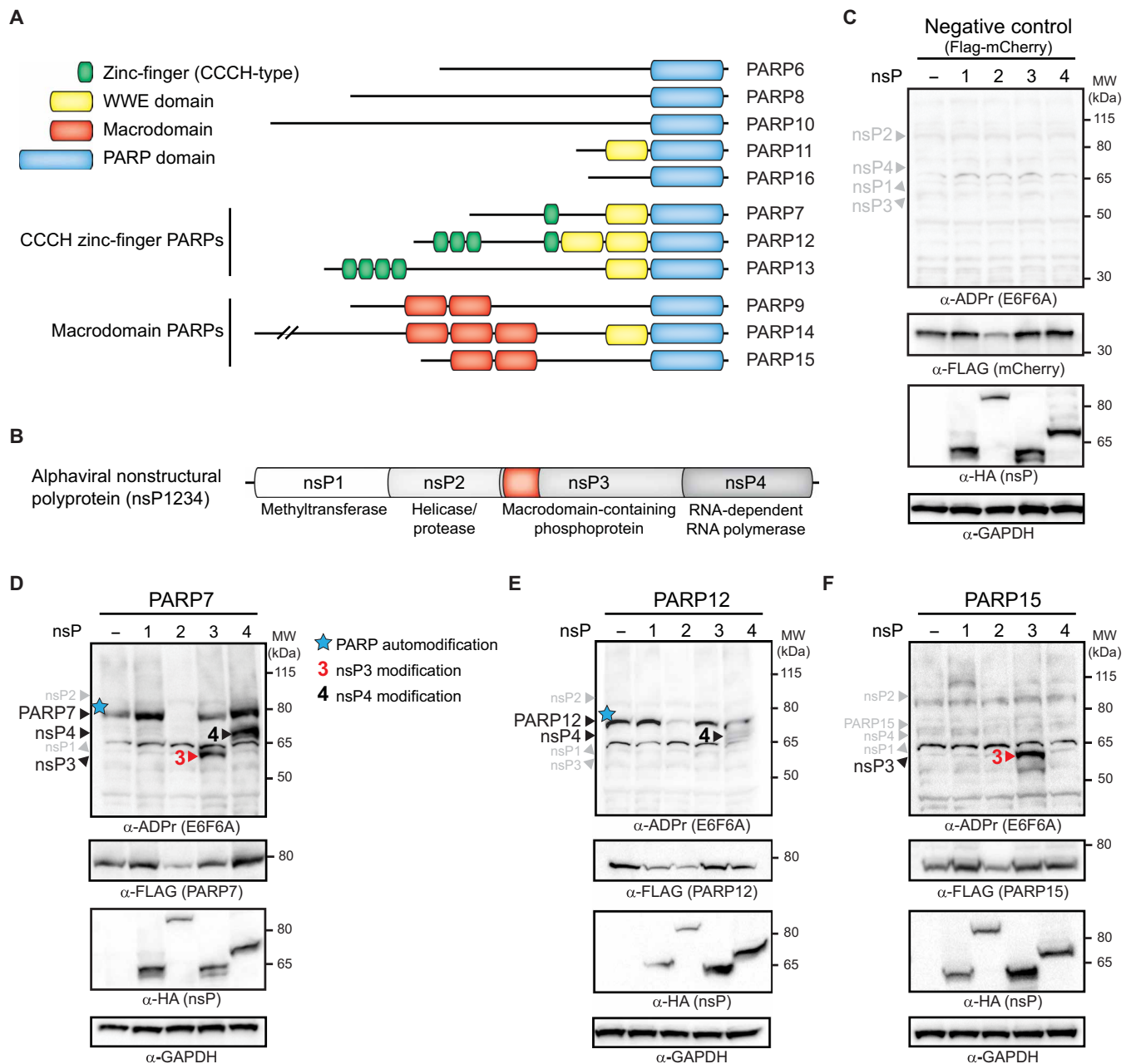
Fig. 1. A subset of human PARP proteins ADP-ribosylates alphavirus nsPs. (**A**) Domain architecture schematics and amino acid lengths of human PARP proteins used in this work. Only the domains shown in the legend are marked on each PARP protein. Domain annotations were obtained from www.uniprot.org. MW, molecular weight. (**B**) Schematic of the alphaviral nsPs that make up the nonstructural polyprotein. Highlighted is the position of the viral macrodomain in nsP3. (**C** to **F**) Western blots probed for ADP-ribosylated proteins with the indicated PARPs and nsPs cotransfected in HEK293T cells. Expected positions of each individual PARP protein and nsP are shown, with those showing no specific ADP-ribosylation indicated in gray and those that are ADP-ribosylated in at least one lane indicated in black. Automodification of PARP7 and PARP12 indicated by blue stars and specific labeling of nsP3 and nsP4 are indicated in the appropriate lanes. Blots with all other PARP proteins are found in fig. S2. The decrease in automodification and FLAG-tagged protein expression in all lanes expressing nsP2 is likely caused by the known role of nsP2 in inhibiting host gene expression (*34*). All blots are representative of at least three independent biological replicate experiments.

macrodomain is catalytically active. We further demonstrate that the antiviral activity of IFN-γ against another alphavirus, SinV, is strongly attenuated when we knock down any member of the CCCH zinc-finger PARP family, including PARP7, PARP12, or the enzymatically inactive PARP13, or through chemical inhibition of PARP7. Last, we reveal that PARP7, PARP12, and PARP13 share a domain architecture

comprising a zinc-finger domain, two tandem WWE domains, and a PARP domain that originated in metazoans and exists across a wide variety of species. Together, these data indicate that the CCCH zinc-finger PARPs are part of an ancient subfamily of PARP proteins that play an important role in the innate antiviral immune response but can be antagonized by the activity of viral macrodomains.

RESULTS

Human PARP7, PARP12, and PARP15 ADP-ribosylate individual viral nsPs

To determine whether any PARPs are able to ADP-ribosylate alphaviral nsPs, we cloned the cytoplasmic MARylating PARP proteins, PARP6 to PARP16, into mammalian expression plasmids (Fig. 1A). PARP9 and PARP13 are the only members of the PARP family that lack critical residues for catalysis (27) but were included because PARP9 has been reported to have some catalytic activity (28) and both have been shown to have either direct or indirect antiviral functions (29–31). The alphavirus nsPs, nsP1, nsP2, nsP3, and nsP4 from SFV (see Fig. 1B), which form the replication complex in the host cell cytoplasm, were likewise cloned into mammalian expression plasmids. All cloned PARPs and SFV nsPs express in human embryonic kidney (HEK) 293T cells, although the protein accumulation varies depending on the exact PARP or nsP construct (fig. S1).

All pairwise combinations of individual PARPs and individual nsPs were then cotransfected into HEK293T cells, and ADP-ribosylation was measured with an ADPr-specific antibody that is capable of recognizing both MARylated and PARylated proteins (antibody E6F6A) (32) (Fig. 1C and fig. S2). Although we observed automodification by several PARPs (Fig. 1, C to F, and fig. S2), as has been described previously (33), we only observed modification of viral nsPs in four cases. Specifically, we observed ADP-ribosylation of nsP3 by PARP7 and PARP15 and modification of nsP4 by PARP7 and PARP12. We further confirmed that viral protein modification mediated by PARP7, PARP12, and PARP15 was MARylation, as they could be detected by a MAR-specific antibody (antibody AbD33204) (fig. S3). In addition to observing the specific ADP-ribosylation signal at molecular weights and conditions that indicate specific viral protein modification, we also confirmed ADP-ribosylation of nsP3 and nsP4 by immunoprecipitating viral nsPs with an anti–hemagglutinin (HA) antibody and subsequently detecting PARP-mediated ADP-ribosylation with both our anti-ADPr antibodies (fig. S4). We observed no specific modification of nsP1 nor did we observe that nsP1 coexpression altered any patterns of automodification. Expression of viral nsP2 caused a general decrease in overexpressed protein levels, including mCherry control and PARP proteins, and a concomitant decrease in automodification levels (Fig. 1, C to F), consistent with the known role of nsP2 in inhibiting host gene expression (34). Although these experiments were performed using overexpressed individual PARPs and nsPs, these biochemical data indicate that a subset of human PARP proteins has the potential to specifically ADP-ribosylate alphavirus nsPs and served as a starting point for further investigation into the function of these specific PARPs and their antagonism by viral macrodomains.

Macrodomain activity reverses host PARP ADP-ribosylation of viral proteins

One unexpected finding from our coexpression data was that the macrodomain-containing nsP3 protein did not reduce the ADP-ribosylation of host or viral targets. The macrodomain from several alphaviral nsP3 proteins has previously been shown to be effective at removing ADP-ribosylation from substrates (35, 36). However, we saw little to no reduction in automodification in samples that contained nsP3 (fig. S2). Moreover, we observed robust modification of nsP3 when coexpressed with PARP7 or PARP15 (Fig. 1, D and F), a result that is again inconsistent with the ADP-ribosylhydrolase activity of nsP3. We therefore hypothesized that the nsP3 we were using

may not be fully active as an ADP-ribosylhydrolase, as we have recently discovered for several other alphavirus macrodomains (36).

Our nsPs were derived from strain SFV4, which was the source strain for many currently used reporter and heterologous alphavirus expression systems (37, 38). We therefore wished to determine whether the SFV4 macrodomain may be distinct from other SFV strains. When comparing the 20 SFV polyproteins found in the nonredundant protein database, SFV4 was unique in having a single amino acid change from alanine to glutamic acid (A48E) within the macrodomain (Fig. 2A). Further investigation of diverse vertebrate-infecting alphaviruses revealed that macrodomain position 48 never contained a charged residue with the exception of SFV4. Moreover, the only other alphaviruses that contain an glutamic acid at that position are insect-specific alphaviruses, such as Eilat virus, that have lost the ability to replicate in vertebrate hosts (39) and lack ADP-ribosylhydrolase activity in the macrodomain (36) (Fig. 2B). To determine whether an A48E change might be predicted to alter macrodomain ADP-ribosylhydrolase activity, we mapped this position on the crystal structure of the Getah virus macrodomain solved in complex with ADPr (Fig. 2C) (40). Although residue 48 is not part of the catalytic core of the macrodomain, it is packed against a critical loop that is involved in substrate binding and catalyzing the removal of ADPr from target proteins (Fig. 2C). We further used AlphaFold2 (41) to predict the structure of the SFV macrodomain, either with an alanine or with a glutamic acid in residue 48 (Fig. 2D). As expected, the presence of the glutamic acid shifts the structure of the loop on which it is present, further supporting the possibility that this substitution may alter macrodomain ADP-ribosylhydrolase activity.

On the basis of this sequence and structural evidence, we hypothesized that a substitution of alanine to the larger and charged glutamic acid at residue 48 could affect macrodomain catalytic activity. We therefore created a variant of our SFV nsP3 protein, E48A, in which the glutamic acid at macrodomain position 48 was changed to an alanine to match all other SFV isolates. We found that this substitution greatly increased the ability of nsP3 to catalyze the removal of PARP10 automodification relative to the original SFV4 nsP3 (Fig. 3A). Moreover, this nsP3 variant catalyzed the removal of PARP10 auto-ADP-ribosylation to almost the same degree as the well-characterized archaeal macrodomain Af1521 (42). We also found that PARP15 is robustly able to ADP-ribosylate SFV4 nsP3 in its original, less enzymatically active form, while the E48A nsP3 shows little to no steady-state modification by PARP15 (Fig. 3B). These data are consistent with a model in which PARP15 ADP-ribosylates nsP3 but that modification can be removed by the active nsP3 macrodomain. Because of the fact that many PARPs can modify proteins on aspartic and glutamic acids (2–5), we next wished to confirm that our E48A substitution did not simply remove the site for PARP15-mediated ADP-ribosylation. We therefore inactivated the macrodomain in the active E48A background by introducing an alanine into the highly conserved N21 position of the macrodomain (36, 43). With this double-substituted nsP3, E48A/N21A, we observed robust PARP15-mediated modification of nsP3, indicating that catalytically inactive nsP3 can be modification regardless of the amino acid at position 48 (fig. S5). We also observed that the active (E48A) macrodomain reduced the steady-state levels of PARP12-mediated ADP-ribosylation on nsP4 when expressed in trans, indicating that the nsP3 macrodomain can reverse ADP-ribosylation on other viral proteins (Fig. 3C). Under these biochemical conditions, we observed that PARP7-mediated automodification and transmodification of
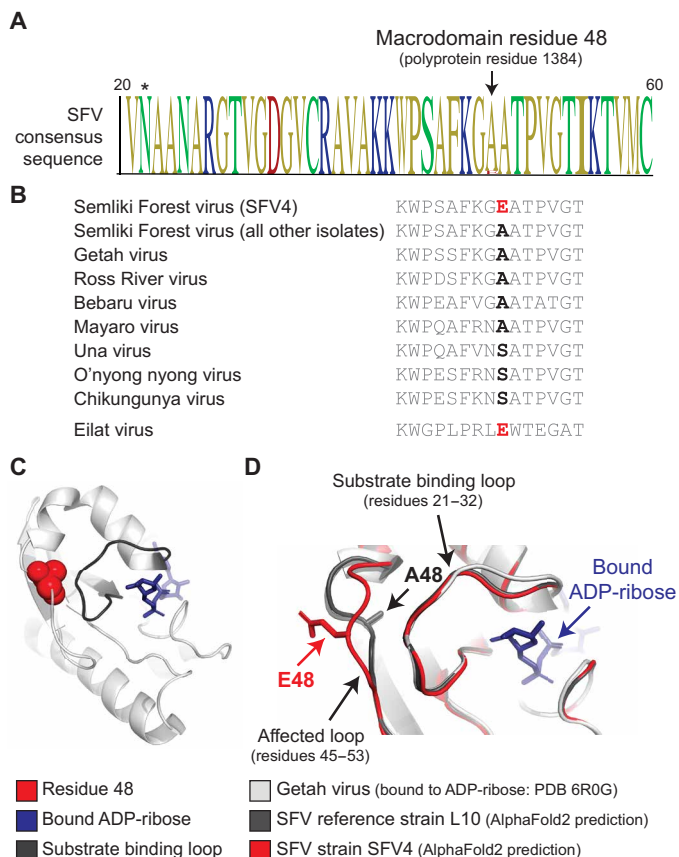
Fig. 2. Evolutionary and functional prediction for altered catalytic activity of the SFV4 macrodomain. (**A**) Consensus motif from an alignment of 20 SFV nsP3 sequences surrounding position 48 (SFV4 numbering), indicating the high conservation of the macrodomain sequence. SFV4 contains the sole difference in this region of the alignment, replacing a well-conserved alanine at position 48 (polyprotein position 1384) with a glutamic acid. A list of all sequences used is found in data S1 (tab 1). The position of the conserved N21 residue used in this manuscript for inactivating macrodomain activity is indicated with an asterisk. (**B**) Alignment of the region surrounding residue 48 from diverse members of the "SFV complex" of alphavirus phylogeny. All members, except SFV4, have an A or S in position 48. Also included is the macrodomain from Eilat virus, an insect-specific virus that lacks the ability to replicate in vertebrate cells (*39*) and that lacks ADP-ribosylhydrolase activity (*36*). Among all alphaviruses, only the insect-specific viruses such as Eilat virus contain an E at position 48. A list of all sequences used is found in data S1 (tab 1). (**C**) Structure of the macrodomain from Getah virus [Protein Data Bank code: 6R0G; (*40*)] bound to ADPr (displayed in blue), showing the position of residue 48 (red) as directly in contact with the ADPr substrate binding loop (residues 21 to 32, displayed in dark gray). (**D**) Structural alignment of the Getah virus macrodomain with AlphaFold2 (*41*) predictions of the macrodomain from SFV4 and the macrodomain from other SFV isolates. The residue 48 side chain is shown as sticks. The loop (residues 45 to 53) that is affected by E48 versus A48 is indicated, as is the substrate binding loop (residues 21 to 32), which contains several conserved residues including N21, N24, and G32.

nsP3 are mostly resistant to removal by the macrodomain-active (E48A) form of nsP3 (Fig. 3D). Although the basis for this biochemical resistance observation remains unknown, PARP7 has previously been shown to ADP-ribosylate cysteines in a manner that would prevent macrodomain-catalyzed hydrolysis (*44*). Alternatively, PARP7 shows some of the highest levels of nsP modification despite showing the lowest level of protein accumulation of all tested PARPs

based on our anti-FLAG Western blot (fig. S1). Such high levels of specific ADP-ribosylation activity may suggest that, in our biochemical assays, macrodomain-mediated removal may not be able to strongly affect the steady-state levels of ADP-ribosylation as detected by our antibodies. Additional virology data (see below) indicate that macrodomain activity can effectively antagonize the activity of PARP7. Overall, these data not only indicate that the SFV4 macrodomain has attenuated enzymatic activity but also support the model showing that alphaviral macrodomain activity can antagonize PARP-mediated ADP-ribosylation of viral proteins.

PARP7, PARP12, and PARP15 inhibit alphavirus replication and are antagonized by viral macrodomain activity

On the basis of our discovery that PARP7, PARP12, and PARP15 ADP-ribosylate viral nsPs and that the viral macrodomain can antagonize this activity, we next wished to determine whether these same PARPs affect SFV replication in a macrodomain-dependent way. To do this, we used the SFV replication reporter from which we isolated our SFV nsPs (*45*) and that we and others have used to study the effect of PARP13 on alphavirus replication (*16*, *46*) (Fig. 4A). In this system, a gene encoding β-galactosidase (LacZ reporter) replaces the viral structural proteins on the viral subgenomic mRNA, allowing the use of β-galactosidase activity as a readout for several steps of the viral replication cycle that are facilitated by viral nsPs, including viral transcription, genome replication, and protein production and processing (*45*). To test the effects of PARP-mediated ADP-ribosylation and viral removal, we created two versions of the SFV replication reporter system. In the first version, we made a "macro active" version in which we introduced the E48A substitution in the macrodomain of nsP3 (Fig. 4B) on the basis of our observation that this substitution increases ADP-ribosylhydrolase activity and is representative of other SFV isolates. In the second version, we made a "macro inactive" SFV replication reporter by introducing an N21A substitution into the macrodomain-active site (Fig. 4B), as we did in data shown in fig. S5. Transfection of the isolated "macro active" and "macro inactive" nsP3s from these viral replication reporters showed the expected ability (macro active) or lack of ability (macro inactive) to catalyze the ADP-ribosylhydrolysis of PARP10 automodification (Fig. 4C).

Despite the fact that attempts to make macrodomain-inactivating substitutions in replication-competent chikungunya virus have previously been shown to rapidly revert to wild type (WT) (*22*), we found that our "macro inactive" reporter system still showed robust replication in HEK293T cells as measured by β-galactosidase activity (Fig. 4D). Moreover, overexpression of either the short or long isoforms on PARP13, which both inhibit replication of alphaviruses in a manner that does not require ADP-ribosylation activity (*16*, *46–48*), is equally effective at inhibiting SFV replication regardless of whether the macrodomain is active or inactive (Fig. 4E). PARP10, which we found does not modify any SFV nsPs in our biochemical assays, shows no antiviral activity relative to conditions in which no PARP is overexpressed. However, consistent with our biochemical data, overexpression of human PARPs that ADP-ribosylate alphaviral nsPs had inhibitory effects that were dependent on the ability of the viral macrodomain to catalyze the removal of ADP-ribosylation. For instance, PARP12 expression had a small but significant inhibitory effect on replication of the "macro active" SFV but a much stronger inhibitory effect against the "macro inactive" SFV (Fig. 4, E and F). Likewise, for PARP15, we observed significant inhibition of replication
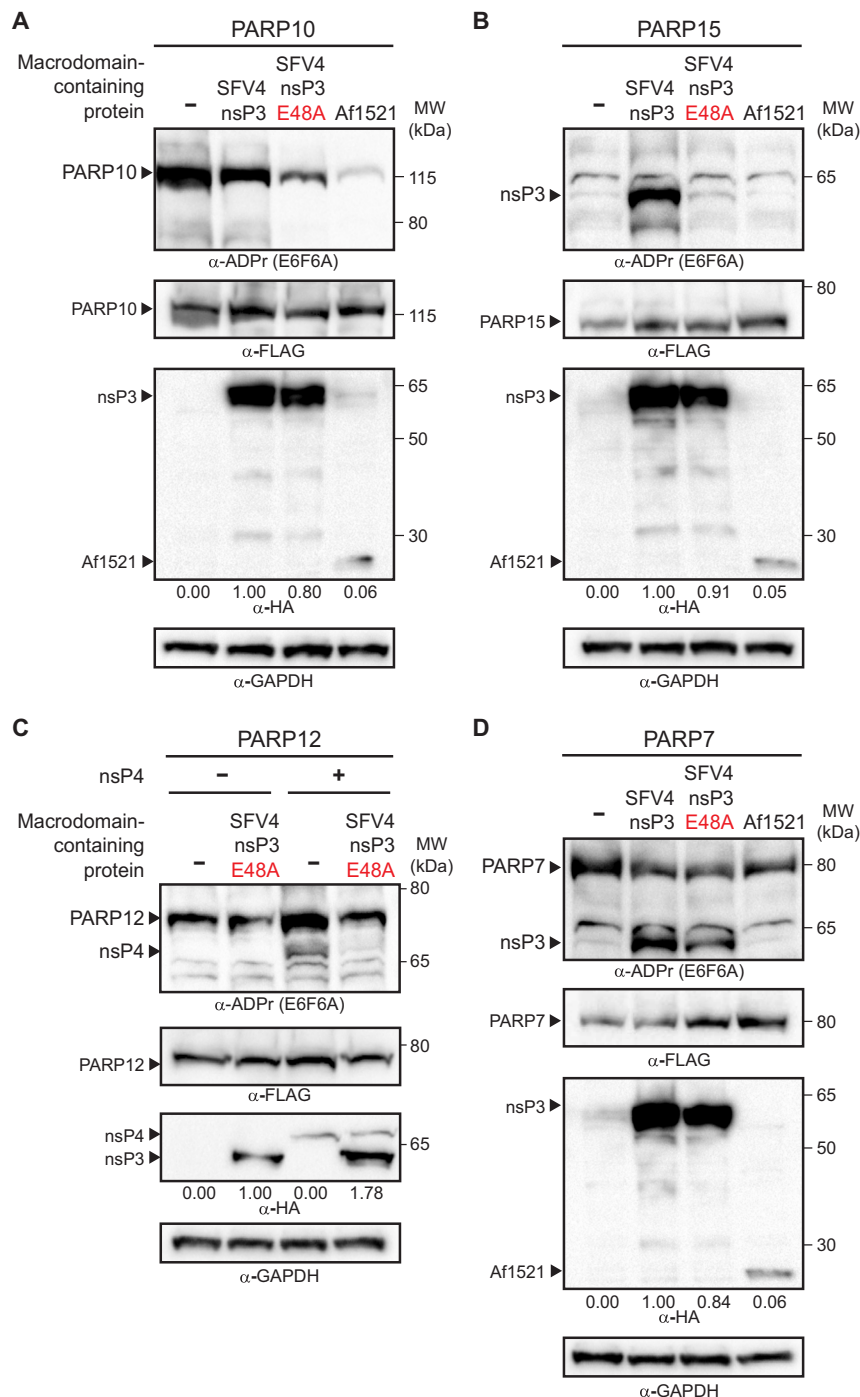
Fig. 3. The macrodomain activity of SFV nsP3 affects PARP-mediated labeling. (**A**) Assay for the ADP-ribosylhydrolase activity of the indicated macrodomain-containing protein. Coexpression of PARP10 with nsP3 from the original SFV4 sequence ("SFV4"), a version in which E48A substitution is introduced ("SFV4 E48A"), or a macrodomain of archaeal origin with high enzymatic activity ("Af1521"). The E48A substitution that restores SFV4 nsP3 to the consensus sequence increases ADP-ribosylhydrolase activity when tested against PARP10. Numbers at the bottom of the anti-HA blot indicate quantification of bands for macrodomain-containing proteins (nsP3 in lanes 2 and 3 and Af1521 in lane 4). (**B**) Coexpression of PARP15 with the indicated macrodomain-containing protein. Unlike the original SFV4 nsP3 protein, co-expression of PARP15 with SFV4 nsP3 E48A shows no accumulation of ADP-ribosylation, consistent with macrodomain-catalyzed removal of the PARP15-mediated ADP-ribosylation. (**C**) Coexpression of PARP12 with SFV nsP3 and nsP4. Coexpression of the active SFV4 nsP3 (E48A) results in a decreased signal of ADP-ribosylation on nsP4, indicative of macrodomain-catalyzed removal of PARP12-mediated ADPr-ribosylation of nsP4. (**D**) Coexpression of PARP7 with the indicated macrodomain-containing protein. PARP7 modification of nsP3 is not as sensitive to macrodomain-mediated removal as PARP15 modification of nsP3. Likewise, Af1521 is less effective at removing PARP7 automodification relative to near-complete removal of PARP10 automodification by Af1521 (A). All experiments were performed in HEK293T cells, and blots are representative of two (C) or three or more (A), (B), and (D) independent biological replicate experiments.
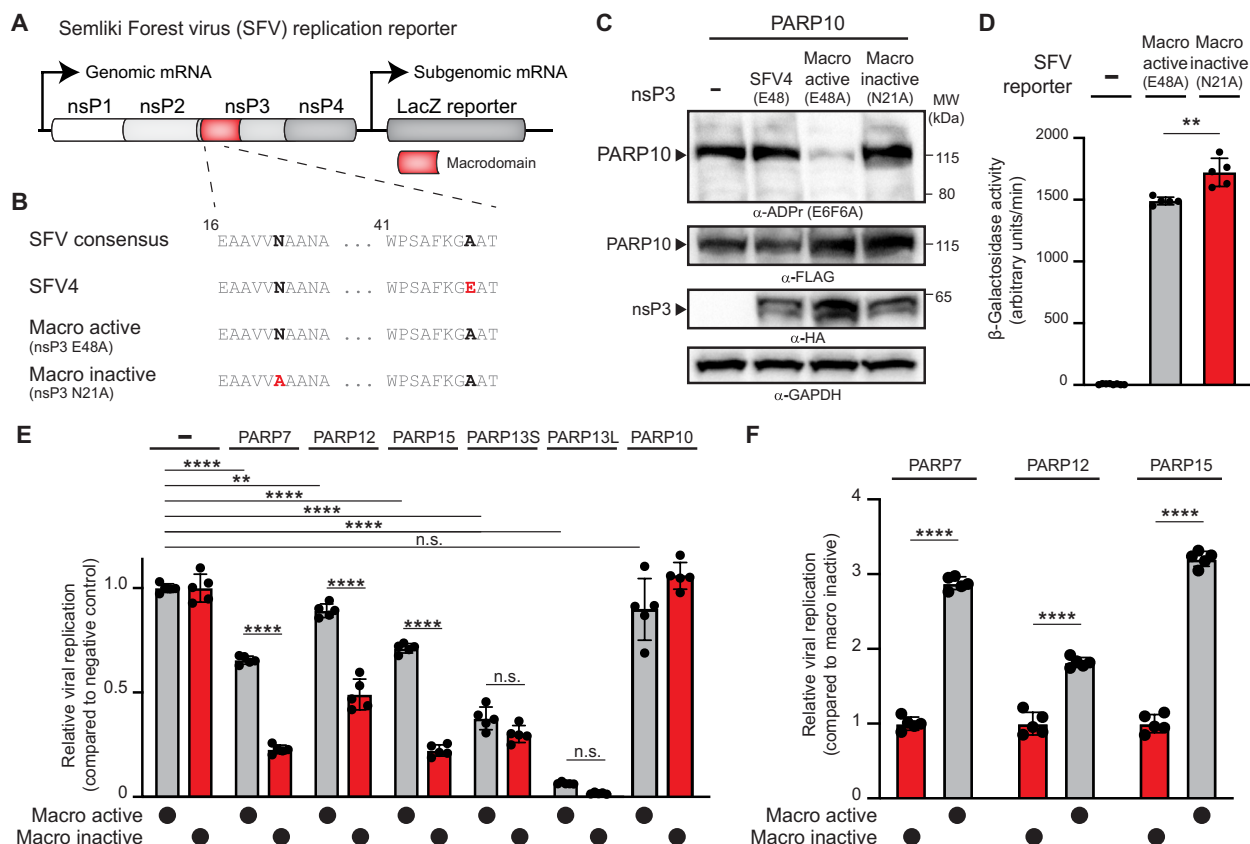
Fig. 4. The macrodomain activity of SFV nsP3 affects PARP-mediated antiviral activity. (**A**) Schematic of the SFV4 β-galactosidase reporter constructs (*45*) used in these studies. (**B**) Macrodomain sequences from the SFV consensus (see Fig. 2A), SFV4, and the "macro active" and "macro inactive" versions used in these studies. (**C**) Assay for ADP-ribosylhydrolase activity of the indicated macrodomain-containing SFV nsP3s on PARP10 automodification in HEK293T cells. Blots are representative of three independent biological replicate experiments. (**D**) β-Galactosidase output of SFV replication reporters with a catalytically active macrodomain ("macro active") compared to catalytically inactive macrodomain ("macro inactive") in HEK293T cells. "−" indicates a condition in which an empty cloning vector (pQCXIP) was transfected in place of the SFV4 reporter. (**E**) SFV4 replication reporters with active or inactive macrodomains tested against a variety of PARP proteins in HEK293T cells. PARP13S (ZAP-S) and PARP13L (ZAP-L) lack a catalytically active PARP domain and thus have anti-alphavirus activity that is independent of ADP-ribosyltransferase activity. In contrast, the antiviral activities of PARP7, PARP12, and PARP15 are dependent on the ADP-ribosylhydrolase activity of the SFV macrodomain. "−" indicates a condition in which a negative control vector expressing 3×FLAG-mCherry was transfected. Under these conditions, no PARP was transiently overexpressed, although HEK293T cells do endogenously express several PARPs (**F**) Normalized fold change of SFV replication with an active versus inactive macrodomain. Data from (E) were normalized for each treatment to the SFV macro inactive condition. (D) to (F) $N = 5$ biological replicates. (D) and (F) Data were analyzed using unpaired Student's *t* tests. (E) Data were analyzed using the two-way ANOVA with Šidák's post test. **$P < 0.01$; ****$P < 0.0001$; n.s., not significant.

of the macrodomain-active SFV; however, the effect of PARP15 over-expression on SFV replication was amplified when the virus encoded an inactive macrodomain (Fig. 4, E and F). We also observed this same potentiated antiviral effect with PARP7 against the macrodomain-inactive SFV replicon despite our biochemical data suggesting that steady-state PARP7-mediated modifications are largely resistant to macrodomain ADP-ribosylhydrolase activity, leaving open the possibility that other macrodomain functions including ADPr-binding could antagonize PARP7 (Fig. 4, E and F). Thus, unlike PARP13, the antiviral effects of PARPs indicate that ADP-ribosylate viral proteins are antagonized by viral macrodomain activity.

Zinc-finger PARPs display anti-alphavirus activity during IFN-γ immune activation

We next asked whether the PARPs that we identified as being able to modify viral proteins, and that we found have antiviral activity when overexpressed, are able to inhibit viral infection when endogenously expressed in the context of immune activation. To do this, we turned to a different alphavirus, SinV, which is a model full-replication competent alphavirus that has been used in studies of PARP13 antiviral activity (*29*, *46–49*) and macrodomain function (*23*, *24*, *50–52*).

We first wished to determine whether the same PARP proteins that modify SFV nsPs also modify SinV nsPs. We therefore created overexpression constructs expressing SinV nsP3 and SinV nsP4. Unlike with SFV4, we observed that the "WT" SinV nsP3 had robust ADP-ribosylhydrolase activity, as we had seen previously with the SinV macrodomain alone (*36*) (Fig. 5A). We therefore also created an nsP3 with an N21A substitution as we did for SFV nsP3 to fully inactivate the ADP-ribosylhydrolase activity of nsP3 (Fig. 5A). Similar to the case with SFV nsP4, we observed robust ADP-ribosylation of SinV nsP4 when coexpressed with PARP7 or PARP12 (Fig. 5B). We observed no PARP7-mediated labeling of either catalytically active or catalytically inactive nsP3, suggesting that nsP3 sequence evolution may shape the ability of this viral protein to be a target for
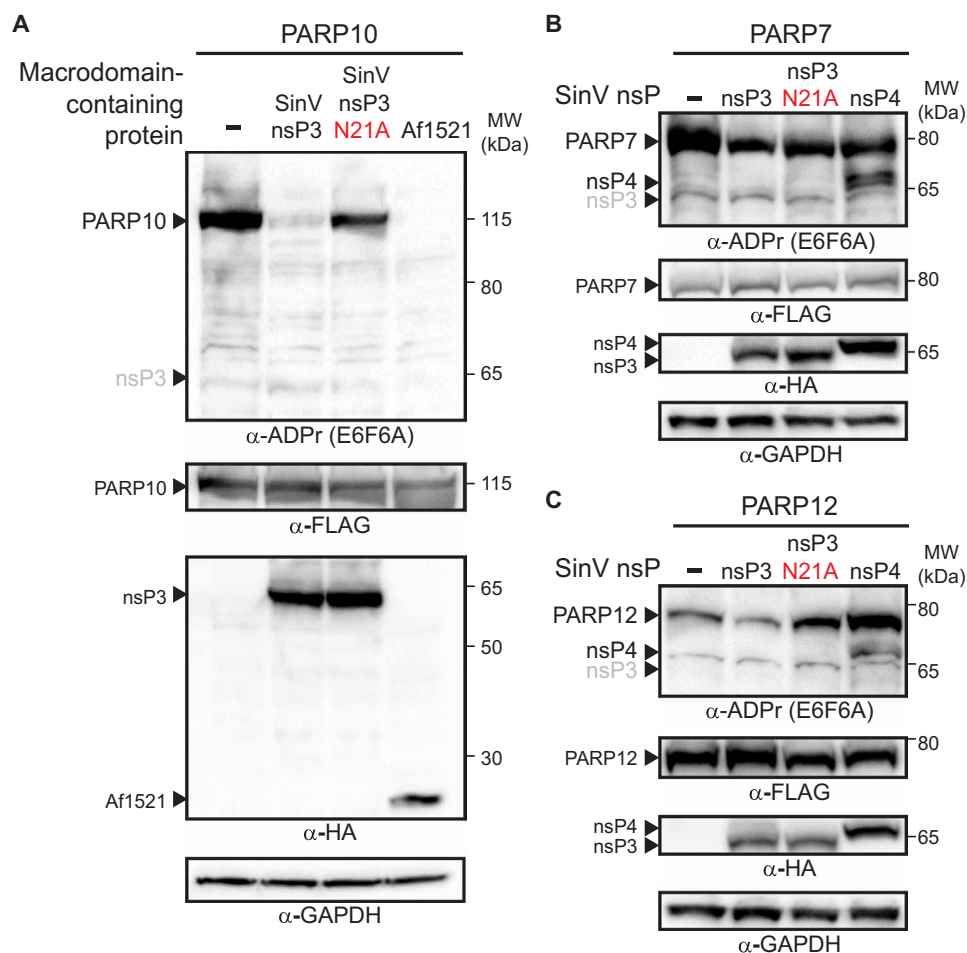
Fig. 5. SinV nsP4 is ADP-ribosylated by PARP7 and PARP12. (**A**) SinV nsP3 contains a macrodomain with ADP-ribosylation activity. The indicated nsP3 (WT or N21A mutant) from SinV, or Af1521, was coexpressed with PARP10. WT nsP3 and Af1521 can reverse PARP10 automodification, but the N21A mutant nsP3 cannot. (**B** and **C**) Overexpression of SinV nsP3 (WT or N21A mutant) or nsP4 with PARP7 (B) or PARP12 (C). No labeling of either version of nsP3 is observed, but nsP4 is modified during coexpression with PARP7 or PARP12. All experiments were performed in HEK293T cells, and blots are representative of at least three independent biological replicate experiments.

PARP7. In spite of the lack of nsP3 labeling, we still hypothesized that PARP7 and PARP12 may have anti-SinV activity similar to their anti-SFV activity based on their ability to ADP-ribosylate SinV nsP4.

We next tested whether endogenous PARP proteins have antiviral activity. To do this, we used human Huh7 cells, which respond robustly to both type I (IFN-α and IFN-β) and type II (IFN-γ), and which we and others have previously used to study the antiviral effects of PARP13 against SinV (*46*, *53*). We therefore infected human Huh7 cells with SinV and used small interfering RNA (siRNA) to knock down the expression of PARP7, PARP12, or the remaining member of the CCCH zinc-finger PARP proteins, PARP13 (fig. S6). Because of the fact that SinV is potently inhibited by IFN-γ (*54*, *55*) and that IFN-γ stimulates cellular ADP-ribosylation (*56–58*), we performed knockdowns with or without pretreatment with IFN-γ. Consistent with these previous reports, we observed an IFN-concentration dependent inhibition of SinV replication, resulting in a 100- to 1000-fold decrease in viral titers at 100 U/ml IFN-γ (Fig. 6, A to C). We found that silencing of any of the zinc-finger PARP proteins, PARP7 (Fig. 6A), PARP12 (Fig. 6B), or PARP13 (Fig. 6C), resulted in partial or complete restoration of viral replication in the presence of IFN-γ.

In contrast, we saw no effect of silencing PARP10 in these assays (fig. S7), consistent with the lack of effect of PARP10 in our SFV reporter assays. In addition, we found that treatment of the cells with the small molecule Phthal01, which inhibits PARP7 but not the other MARylating PARPs at the concentrations used (*44*) (fig. S8), attenuates the antiviral effects of IFN-γ against SinV (Fig. 6D). We only observed this PARP-specific antiviral effect when the innate immune response was stimulated with IFN-γ but not IFN-α and not when we inhibited PARP1/PARP2 with a known specific inhibitor of those proteins (*59*) (Fig. 6E). These data thus reveal a role for all three zinc-finger PARP proteins in IFN-γ–dependent antiviral activity against alphaviruses.

Zinc-finger PARPs contain an ancient protein architecture involved in antiviral defense

Our data above revealed that all three human CCCH zinc-finger domain containing PARPs can inhibit alphavirus replication (Fig. 4) and are important for IFN-γ–mediated antiviral activity (Fig. 6) in human cells. We therefore wished to determine what molecular features are conserved among these three proteins and how broadly zinc-finger PARP proteins are represented across the tree of life.
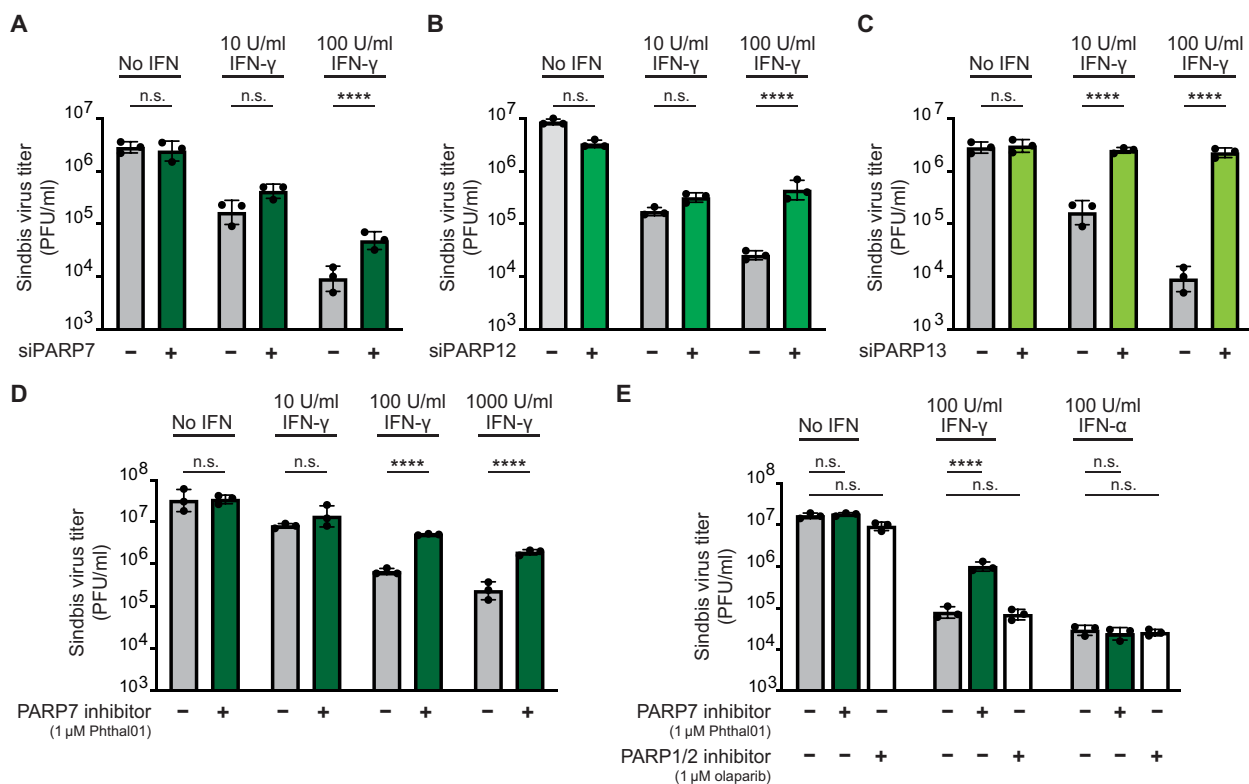
Fig. 6. Zinc-finger PARPs, PARP7, PARP12, and PARP13, are important for the antiviral activity of IFN-γ. (**A** to **C**) Human Huh7 cells were pretreated with the indicated siRNA and concentration of IFN-γ and then infected with SinV (25,000 PFU per well; multiplicity of infection of ~0.1). Negative control conditions ("−") were treated with a nontargeting negative control siRNA. siRNA silencing of either PARP7 (A), PARP12 (B), or PARP13 (C) attenuates the antiviral effects of IFN-γ against SinV replication. (**D** and **E**) Human Huh7 cells were treated with the PARP7-selective inhibitor Phthal01, the PARP1/2 inhibitor olaparib (*59*), or dimethyl sulfoxide control and the indicated concentration of IFN-γ or IFN-α and then infected with SinV. (A) to (E) *N* = 3 biological replicates. Data were analyzed using the two-way ANOVA with Šidák's post test. ****$P < 0.0001$; n.s., not significant.

We first wished to determine what conserved protein architecture exists between PARP7, PARP12, and PARP13. On the basis of existing annotations (Fig. 1A), each of these human PARP proteins contains at least one CCCH-type zinc-finger domain, at least one WWE domain, and a PARP domain. In addition to those annotated domains, aligning human PARP7, PARP12, and PARP13 revealed a clear conservation that overlaps the C-terminal zinc-finger domain and two WWE domains that are annotated in PARP12 (Fig. 7A). Further analysis revealed that the residues that are important for the zinc-finger domain and both WWE domains are conserved across these proteins (*60*) (Fig. 7B). Notably, recent structural data on PARP13 indicate that this tandem configuration of a zinc-finger domain followed by two WWE domains forms a single structural unit that can bind to PAR and potentiates the antiviral activity of PARP13 (*60*). These data indicate that this putative PAR-binding module (zinc-finger-WWE-WWE), followed by a PARP domain, characterizes this subgroup of human PARP proteins (Fig. 7C). Notably, the other two PARPs that contain WWE domains, PARP11 and PARP14 (Fig. 1A), only contain a singular WWE domain rather than the zinc-finger-WWE-WWE architecture found in the PARP7, PARP12, and PARP13 subgroup.

We next searched for this domain architecture throughout eukaryotic and prokaryotic genomes. By performing iterative sequence homology searches with PSI-BLAST, as well as domain architecture searches using InterPro (see Materials and Methods), we found that this PAR-binding-PARP domain architecture only exists in certain metazoan lineages and is notably lacking from nonmetazoan eukaryotes and hexapods (e.g., insects) and nematodes (e.g., *Caenorhabditis elegans*) (Fig. 7D). Using phylogenetic analyses, we were able to clearly identify a clade of vertebrate PARP7-like proteins and a clade of vertebrate PARP12/13–like proteins. In addition, several other metazoan lineages, including cnidarians (e.g., corals and anemones), echinoderms (e.g., starfish), spiralians (e.g., mollusks), and crustaceans (e.g., crabs), have proteins containing a PAR-binding-PARP domain architecture, often with additional zinc-finger domains that are characteristics of vertebrate PARP12/13–like proteins (Fig. 7E). The two PAR-binding-PARP domain proteins in the sea anemone *Nematostella vectensis* (protein accession XP_048581669.1 and XP_001636351.2) are encoded by two of the most up-regulated genes in response to 2,3-cyclic guanosine monophosphate-adenosine monophosphate, a potent activator of antiviral immunity in both cnidarians and mammals (*61*). Together, these results indicate that human PARP7, PARP12, and PARP13 shared an ancient domain architecture that is associated with antiviral immunity across a vast range of metazoan evolution.

DISCUSSION

Increasing evidence indicates that ADP-ribosylation plays an important role at the intersection of viral replication and host antiviral immunity. While a variety of genetic, evolutionary, and virology
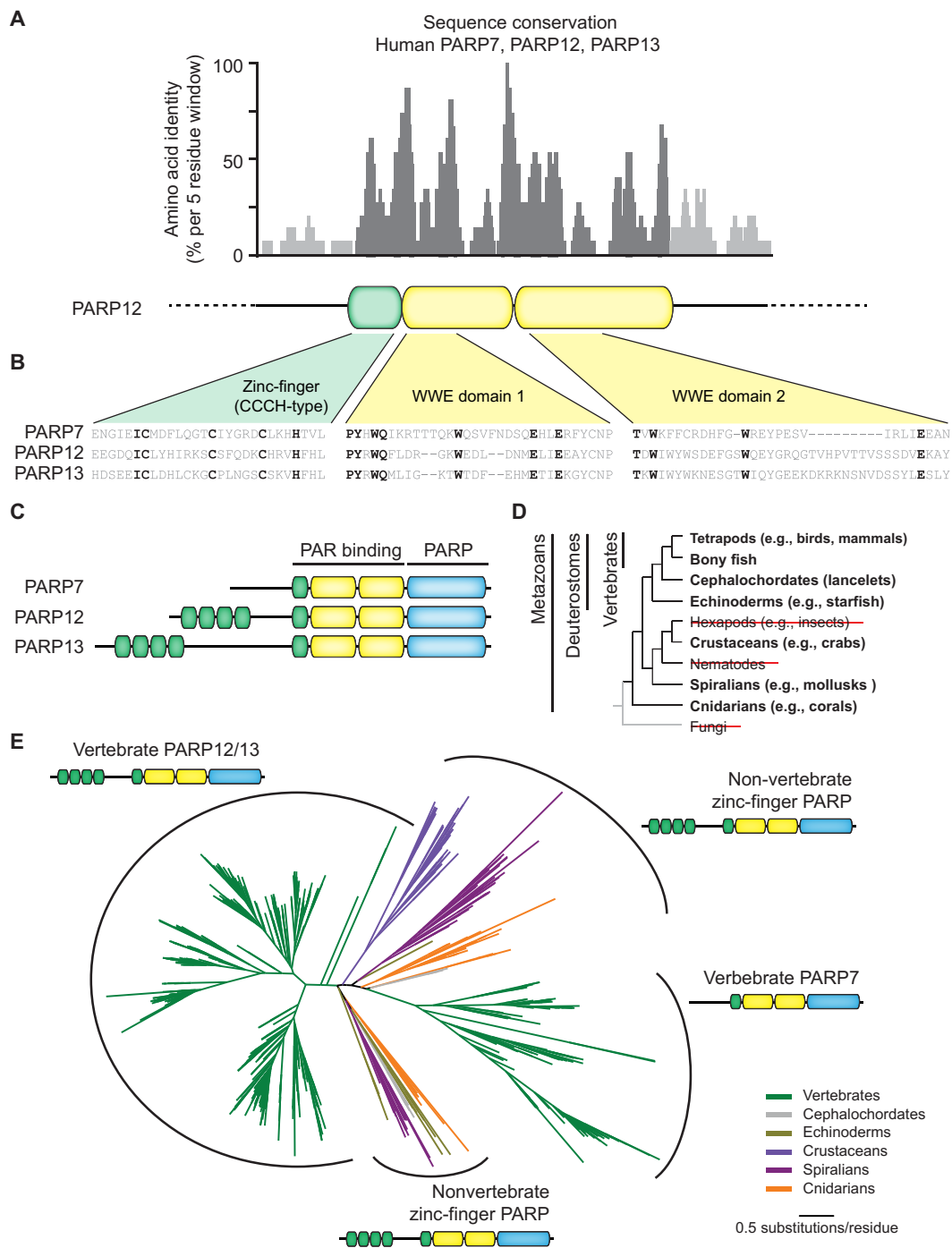
Fig. 7. Ancient domain architecture involved in antiviral immunity. (**A**) Conservation of a zinc-finger and tandem WWE domain architecture across human PARP7, PARP12, and PARP13. Sliding window analysis of amino acid conservation across the three indicated human PARPs. A schematic of PARP12 is shown below to indicate the positions of the annotated zinc-finger and WWE domains (**B**). Amino acid alignments of the indicated human PARPs in the indicated protein regions. Residues in bold are conserved across all three proteins and define the CCCH-type zinc-finger and WWE domains. (**C**) Updated domain architecture of PARP7, PARP12, and PARP13 based on amino acid conservation in the indicated domains. Annotation of the PAR-binding domain, comprising a zinc-finger domain followed by two WWE domains, is based on structural and functional analyses performed in PARP13 (*60*). Colors of domains are as in Fig. 1A. (**D**) Presence of the PAR-binding-PARP domain architecture within eukaryotic genomes. Species clades in which one or more proteins with a PAR-binding-PARP domain architecture are present as shown with bold black text. Clades in which no proteins exist with that architecture are shown in black with red strikethrough. (**E**) Phylogeny of metazoan proteins that contain a PAR-binding-PARP domain architecture. Vertebrate PARP7 and PARP12/13 proteins are shown in green, with the corresponding domain architecture shown. Nonvertebrate metazoan proteins, which generally have a PARP12/13 protein architecture, are shown in colors that correspond to the species clade.

studies supports a function for ADP-ribosylation in the immune response and for viral macrodomains in opposing host immunity (*8–12*), the exact molecular players in this conflict over ADP-ribosylation have remained mostly elusive. To begin to address these questions, here, we set out to determine whether any human PARPs could specifically modify alphavirus proteins, whether alphavirus macrodomains could remove those modifications, and whether human PARPs that could modify viral proteins are components of the antiviral immune response against alphaviruses.

First, we used biochemical assays to reveal that three human PARPs, PARP7, PARP12, and PARP15, can specifically modify nsPs, nsP3 and nsP4, from the model alphavirus, SFV. By coexpressing these proteins in human cells, we find robust modification that is both PARP and viral protein specific and have band intensities similar to those seen with PARP automodification. Although these positive results indicate a clear PARP-mediated nsP modification, it is worth noting that the absence of obvious labeling by this method does not eliminate the possibility that other PARP-mediated nsP modifications may occur at levels below our limit of detection. We similarly found that PARP7 and PARP12 can label nsP4 from a related alphavirus, SinV. These data indicate that PARP7 and PARP12 share the ability to ADP-ribosylate the viral nsP4 protein across diverse alphaviruses, likely as a result of the strong degree of conservation of the nsP4 protein that encodes the viral RNA-dependent RNA polymerase.

There are important limitations to these biochemical data, which we viewed as a first step in identifying PARP activities that may be directly antagonized by viral macrodomains. First, our analyses rely on overexpressed PARPs and overexpressed individual viral proteins. During infection, viral nsPs are expressed together, first as a polyprotein and then assembled into replication complexes, and accumulate to lower levels than we are expressing them here. Moreover, structural viral proteins, which are not considered here, are also expressed during infection. Our biochemical assays do not mirror this viral context of these viral nsPs and structural proteins. As such, while we can conclude that the modifications that we describe are possible, detection of modification of viral proteins during infection by human PARPs will be an important next step in studies on PARP-mediated antiviral immunity.

Despite these limitations, we find that the same PARPs that modify SFV-overexpressed nsPs also inhibit replication of a SFV viral reporter. Although the exact mechanism by which these PARPs lead to viral inhibition requires further study, ADP-ribosylation is known to have a variety of modulatory functions, including disrupting protein-protein and protein-RNA interactions and promoting protein degradation (*1–5*). Alternatively, despite the concordance of PARPs that modify viral proteins and PARPs that we find inhibit SFV replication, it is possible that the antiviral functions of PARP7, PARP12, and PARP15 rely on modification of host proteins or host or viral RNA. Additional point mutations that eliminate ADP-ribosylation of viral nsPs will be needed to validate the role of nsP ADP-ribosylation for the antiviral activity of PARP7, PARP12, and PARP15. However, we find that the macrodomain activity of the virus being tested has a critical impact on the efficacy of the antiviral effects of PARP7, PARP12, and PARP15. For instance, PARP12 has a minimal (~10%) inhibitory effect on replication of a variant of SFV that has a fully active macrodomain but has a substantial (>50%) inhibitory effect on replication of a macrodomain-mutant SFV reporter. These results, which correlate with the biochemical data showing that an active

macrodomain can reverse the PARP12-mediated ADP-ribosylation of viral nsP4, further support a model in which viral macrodomain activity has evolved to reverse the inhibitory effects of host antiviral PARPs. These data are also consistent with a recent in vivo data in mice that show that PARP12 is a critical player in the antiviral immune response against a coronavirus in which the macrodomain has been inactivated (*26*). More unexpected was our data indicating that the PARP7-mediated antiviral effect was potentiated by viral macrodomain inactivation. On the basis of our biochemical data showing that PARP7 automodification and transmodification of nsP3 were resistant to macrodomain-mediated removal, we initially predicted that PARP7 antiviral activity would also be largely resistant to viral macrodomain activity. In contrast, we observed that a macrodomain-active SFV replicated to nearly threefold higher levels than a macrodomain-inactive SFV in the presence of PARP7 (Fig. 4F). Although in-depth analysis of PARP7 biochemical activity on specific targets during viral infection, as well as macrodomain activity, will be required to reconcile our biochemical and viral replication data, our results together indicate that macrodomains can antagonize the antiviral activity of PARP7, PARP12, and PARP15.

Such an inference about viral macrodomains antagonizing antiviral PARPs would suggest that macrodomain enzymatic activity would therefore be highly conserved. We recently discovered the recurrent loss of macrodomain ADP-ribosylhydrolase activity in several independent lineages of alphaviruses (*36*). In addition to those examples, we now find that one isolate of SFV, SFV4, also has a macrodomain with attenuated ADP-ribosylhydrolase activity, which further supports the unexpected lack of conservation of full enzymatic activity in alphaviruses. However, the discovery that SFV4 contains a catalytically attenuated macrodomain has potential implications beyond the work described here. SFV4 was one of the first enveloped viruses from which a molecular clone was created and was subsequently used to create a system for heterologous protein expression that has been used for more than 30 years (*62*). Consequently, this system, commonly referred to as pSFV1 or its derivatives, has been used as a platform for the development of a variety of heterologous expression, vaccine development, and antitumor delivery systems (*38*, *63–66*). Although our data indicate that macro active and macro inactive reporters replicate equally well in HEK293T cells, we expect that the macrodomain hypomorph that exists in SFV4 may affect the efficacy of some of these SFV4-based heterologous delivery systems when used in an in vivo setting in which the innate immune response is expected to be active. Despite other evidence that supports a requirement for macrodomain activity in replication of alphaviruses including chikungunya and SinVs even in the absence of IFN stimulation (*21*, *22*, *24*, *50*), these data on SFV4 and our previous data on other alphaviral macrodomains (*36*) indicate that full macrodomain enzymatic activity may not be universally required. One important point that may distinguish these effects is that the viral macrodomain "function" likely encompasses many different biochemical activities (*1*, *6*, *8*, *17*). These potentially separable activities include ADP-ribosylhydrolase activity to remove MAR from a target protein, which is the activity that we are measuring in this study, but also bind to both MAR and PAR and ADP-ribosylhydrolase activity that reduces the sizes of PAR chains (e.g., PAR hydrolase activity) (*50*). As such, it is possible that certain activities, such as MAR ADP-ribosylhydrolase activity, are dispensable for some viruses, but other activities are required, and that requirements between alphaviruses, coronaviruses, and other macrodomain-containing viruses will differ.

Further research into the viral macrodomain sequence and functional diversity among and within viral groups will likely reveal subtly which substitutions are tolerated, and which viruses can tolerate them, to shed light on the constraints on this important viral enzymatic activity.

We find that PARP7 and PARP12 not only modify alphavirus proteins and inhibit replication of our SFV reporter system but are also important for the IFN-γ–mediated innate antiviral immune response. Using knockdown or chemical inhibition, we find that PARP7 and PARP12 are each important for inhibition of SinV after IFN-γ pretreatment. Although we did not test for effects of PARP15 on the basis of the fact that it is primarily expressed in immune cells (expression data from www.proteinatlas.org), we did also test the effect of knockdown of the third zinc-finger PARP, PARP13. These data, which revealed that PARP13 knockdown entirely eliminates the anti-alphaviral activity of IFN-γ (Fig. 6C), further support the involvement of the entire zinc-finger PARP subfamily in the antiviral effects of IFN-γ. Additional studies will be required to determine the mechanistic link between IFN-γ– and PARP-mediated antiviral effects, especially in light of recent data that revealed that macrodomain mutant SARS-CoV-2 is highly sensitive to the antiviral effects of IFN-γ (67) and that overall levels of ADP-ribosylation in the cell are increased upon IFN-γ treatment (56–58). Clearly, there is an important connection between IFN-γ, PARP-mediated ADP-ribosylation, and antiviral immunity that warrants additional study.

Last, it is notable that the PARPs we find are important for the IFN-γ antiviral response; PARP7, PARP12, and PARP13 comprise a single, ancestrally related subfamily of PARPs. Our evolutionary analyses indicate that these PARPs are characterized by a domain architecture that contains a zinc-finger domain followed by two WWE domains, recently characterized in PARP13 as a single structural unit able to bind PAR (60), followed by a PARP domain. The conservation of this putative PAR-binding domain in this subfamily of antiviral PARPs may provide a link between increased PAR upon immune stimulation (56–58) and their role in the antiviral response, although we have yet to confirm that PARP7 and PARP12 can bind to PAR through their Znf-WWE-WWE domain. Such a model showing that PARP7 and PARP12 can ADP-ribosylate viral proteins and may be able to bind to ADP-ribosylated substrates, and that PARP13 lacks the ability to ADP-ribosylate but requires PAR-binding for its antiviral activity (60), suggests that ADPr addition and recognition may serve as a positive feedback loop to facilitate antiviral activity. PARP7 ADP-ribosylates PARP13 (44), revealing the possibility that PARP7, PARP13, and possibly PARP12 function synergistically together during the IFN-γ antiviral response. Such combined antiviral effects of PARPs have been previously observed during coronavirus infection (25). Consistent with a model in which PARP7, PARP12, and PARP13 function together, the ancestral domain configuration of PAR-binding-PARP has been duplicated and subfunctionalized across different metazoans, potentially providing different configurations of this synergistic antiviral complex. For instance, PARP12 and PARP13 are recently duplicated paralogs of each other (68) in which PARP13 has lost catalytic activity and PARP7 lacks the RNA-binding zinc-finger domains that exist in vertebrate PARP12/13 and in ancestral metazoan proteins in this gene family. Such changes in paralog number, domain structure, and enzymatic activity are characteristic of host genes involved in host-virus evolutionary arms races, including other PARPs (15, 36, 69). Despite these evolutionary innovations, the two PARP12-like paralogs that exist in the cnidarian

N. vectensis are up-regulated along with other immune genes by the same chemical signal that activates the innate immune response in humans (61), suggestive of conservation of the antiviral role of zinc-finger PARPs across a broad range of metazoans. Thus, together, our work reveals a direct molecular conflict between zinc-finger PARPs and viral macrodomains, a critical role for zinc-finger PARPs in the human IFN-γ–mediated antiviral immune response, and a deep conservation of zinc-finger PARP structure and function that predicts their broader antiviral function throughout metazoan evolution.

MATERIALS AND METHODS
Plasmids and constructs
For PARP overexpression, coding sequences of PARP6, PARP7, PARP8, PARP9, PARP10, PARP11, PARP12, PARP13S, PARP13L, PARP14, PARP15, and PARP16 were cloned into the pcDNA5/FRT/TO backbone (Thermo Fisher Scientific, Waltham, MA) with an N-terminal mCherry, P2A linker, and 3×FLAG epitope tag. For SFV nsP overexpression, the nsP1, nsP2, nsP3, and nsP4 sequences were cloned from the SFV4 reporter system pSMART-LacZ-2B (45) into the pQCXIP backbone with an N-terminal HA tag. SinV nsPs nsP1, nsP2, nsP3, and nsP4 were amplified from the infectious clone SINV TE/5'2J-GFP (29) (a gift from C. Rice, Rockefeller University) and cloned into the pQCXIP vector backbone (Takara Bio, San Jose, CA) with an N-terminal HA tag. Single-point mutations to create catalytically active and inactive mutants of macrodomain constructs were performed using overlapping stitch polymerase chain reaction (PCR). All inserts were fully sequenced to verify that no mutations arose during cloning.

Cell culture and transient transfection
Human immortalized cell lines (HEK293T or Huh7) were routinely tested for mycoplasma infection using a PCR kit and kept at a low passage number. HEK293T cells were obtained from American Type Culture Collection (Manassas, VA), and the Huh7 cells were a gift from R. Savan (University of Washington). Cells were grown in complete media using Dulbecco's modified Eagle's medium (Gibco, Billings, MT) with 10% (v/v) fetal bovine serum (Peak Serum, Wellington, CO) and 1% (v/v) penicillin/streptomycin (Invitrogen, Carlsbad, CA). For transient transfections (coexpression, ADPr analysis, and SFV replication assays), HEK293T cells were seeded a day before transfection in a 24-well plate with 500 μl of media per well such that they would be at 60% confluency the following day for transfection. Cells were transfected using 500 ng of total plasmid DNA with 1.5 μl of Transit-X2 transfection reagent (Mirus Bio, Madison, WI) in 100 μl of Opti-MEM (Invitrogen) per well.

Immunoblotting
ADP-ribosylation assays were performed as previously described (36). Briefly, HEK293T cells were transfected in 24-well plates with 100 ng of plasmid expressing the indicated viral nsP and 250 ng of plasmid expressing the indicated PARP. Cells were harvested 20 hours after transfection. As has been previously used (44), we added veliparib (VWR, Radnor, PA), a selective PARP1/PARP2 inhibitor (70, 71), to culture media to a 1 μM final concentration 1 hour before harvest to inhibit PARP1 activity and therefore reduce background PARP1-mediated ADP-ribosylation. At the time of harvest, media were aspirated, phosphate-buffered saline (PBS) was added to cells and aspirated, and then plates were frozen at −80°C. After at least 1 hour

at −80°C, plates were thawed on ice for 10 min and 75 µl of ADPr lysis buffer [50 mM tris (pH 7.4), 150 mM NaCl, 1 mM MgCl$_2$, 1% (v/v) Triton X-100, 1× protease inhibitor (Sigma-Aldrich, St. Louis, MO), 1 µM PDD00017273 (PARG inhibitor, Sigma-Aldrich), 1 µM veliparib, and 1 mM dithiothreitol] was added to each well. After 10 min of incubation on ice, lysates were transferred and centrifuged at 10,000g at 4°C for 5 min. The resulting supernatant was transferred to a new tube, and 4× NuPAGE LDS sample buffer (Invitrogen) containing 5% (v/v) β-mercaptoethanol (VWR) was added. Samples were heated to 95°C for 10 min and briefly centrifuged before being loaded onto a 4 to 12% bis-tris SDS–polyacrylamide gel electrophoresis gel (Invitrogen) and electrophoresed in 1× Mops (Invitrogen) running buffer. Samples were then wet transferred onto a nitrocellulose membrane and blocked with PBS-T containing 5% (w/v) bovine serum albumin for 1 hour. This was followed by incubation overnight at 4°C with primary antibodies for mono/poly-ADPr [anti-poly/mono-ADPr antibody, E6F6A, Cell Signaling Technology, Danvers, MA; (32)], mono-ADPr (Mono-ADP-Ribose antibody, AbD33204, Bio-Rad), anti-FLAG M2 (Sigma-Aldrich), anti-HA (Sigma-Aldrich), or anti-GAPDH (Cell Signaling Technology). Membranes were then rinsed three times in PBS-T and then incubated with the appropriate horseradish peroxidase–conjugated secondary antibodies (Thermo Fisher Scientific, Pittsburg, PA). Membranes were then rinsed three times in PBS-T, and developed with SuperSignal West Pico PLUS Chemiluminescent Substrate (Thermo Fisher Scientific), and imaged on a Bio-Rad GelDoc (Bio-Rad, Hercules, CA). Information on biological replicates is indicated in each figure legend.

Immunoprecipitation of HA-tagged nsP3 and nsP4

HEK293T cells were transfected in six-well plates with 1000 ng of plasmid expressing PARP7 and 1000 ng of plasmid expressing the indicated viral nsP from SFV4. Cells were harvested 20 hours after transfection. One hour before harvesting cells, veliparib (VWR) was added to culture media to a final concentration of 1 µM to inhibit PARP1 activity. At the time of harvest, PBS was added to cells and aspirated, and the plate was then frozen at −80°C. After at least 1 hour at −80°C, plates were thawed on ice for 10 min and 500 µl of ADPr lysis buffer [50 mM tris (pH 7.4), 150 mM NaCl, 1 mM MgCl$_2$, 1% (v/v) Triton X-100, 1× protease inhibitor (Sigma-Aldrich, St. Louis, MO), 1 µM PDD00017273 (PARG inhibitor, Sigma-Aldrich), 1 µM veliparib, and 1 mM dithiothreitol] was added to each well. After 10 min of incubation on ice, lysates were transferred and centrifuged at 10,000g at 4°C for 5 min. After centrifugation, 50 µl of lysate was transferred to a new tube, mixed with 50 µl of 2× NuPAGE LDS sample buffer (Invitrogen), and heated to 97°C for 5 min to serve as "Input" control samples for immunoblots. The remaining 450 µl of lysate was then transferred to Protein LoBind tubes (Eppendorf SE, Hamburg, Germany), and 40 µl of 1:1 (antibody:lysis buffer) monoclonal anti-HA agarose antibody (Sigma-Aldrich, A2095) bead mix was added to each tube. Lysates and beads were then incubated on a rotator for 3 hours at 4°C. Following incubation, samples were washed three times by centrifuging at 800g, discarding the supernatant, and adding 1 ml of fresh ADPr lysis buffer. After the final wash, the supernatant was discarded and 100 µl of 2× NuPAGE LDS sample buffer (Invitrogen) containing 5% (v/v) β-mercaptoethanol (VWR) was added to the beads. Samples were heated to 97°C for 5 min and briefly centrifuged before being loaded, along with "Input" samples from above, onto a 4 to 12% bis-tris SDS–polyacrylamide gel electrophoresis gel (Invitrogen) and electrophoresed in 1× Mops (Invitrogen) running buffer. Immunoblots for mono/poly-ADPr, mono-ADPr, FLAG, HA, and glyceraldehyde-3-phosphate dehydrogenase (GAPDH) were performed as described above.

SFV replication reporter assays

For SFV replication assays, pSMART-LacZ-2B was mutated to either have an active macrodomain (E48A in macrodomain numbering and E1384A in polyprotein numbering) ("macro active") or have an inactive macrodomain [N21A (N1357A) in the context of the E48A (E1384A) substitution] ("macro inactive"). To measure SFV replication activity, 200 ng of the above pSMART-LacZ-2B constructs was cotransfected with 300 ng of PARP expression plasmids into HEK293T cells. SFV replication reporter assays were performed with five wells per condition, where the corner wells of each plate were left untransfected to minimize plate edge effects. Twenty hours after transfection, plates were freeze-thawed three times and then 4-methylumbelliferyl β-D-galactopyranoside (MUG, Thermo Fisher Scientific) was added to each well to a final concentration of 150 µg/ml. The plates were then read for maximal change in fluorescence emission over 15 time points (5 min) with an excitation wavelength of 380 nm and an emission wavelength of 450 nm. Information on biological replicates is indicated in each figure legend.

Viral stocks and viral infections

GFP (green fluorescent protein)–expressing SinV was generated by in vitro transcription from SINV TE/5′2J-GFP, electroporated into BHK cells, and further amplified on BHK cells as previously described (29). All SinV samples were titrated on BHK cells by infecting cells for 90 min; replacing the media with an overlay of Dulbecco's modified Eagle's medium, fetal bovine serum complete medium, and 0.6% (w/v) carboxymethylcellulose; and staining with crystal violet the following day.

For viral infections of Huh7 cells, cells were plated in 24-well plates and infected the following day with 25,000 plaque forming units (PFUs) of SinV, corresponding to a final multiplicity of infection of ~0.1 based on estimates of ~250,000 cells per well at the point of infection. Infections were allowed to proceed for 20 hours before the supernatant was harvested and frozen at −80°C. This supernatant was later titrated to determine PFU-per-well values for each condition. Where indicated, IFN-γ (BioLegend) or IFN-α (Abcam) was added 8 hours before viral infection. For infections involving the PARP7-selective inhibitor Phthal01 (a gift from M. Cohen, Oregon Health Sciences University) (44) and the PARP1/2 inhibitor olaparib (59), the drug or dimethyl sulfoxide control was added 1 hour before IFN induction. Information on biological replicates is indicated in each figure legend.

siRNA treatment and RT-qPCR

Huh7 cells were grown in a six-well plate, with at least two wells being used for each siRNA condition. Dicer-substrate siRNA (DsiRNA) against PARP7 (hs.Ri.TIPARP.13.2), PARP10 (hs.Ri.PARP10.13.2 and hs.Ri.PARP10.13.3), and PARP13 (hs.Ri.ZC3HAV1.13.1) were obtained from Integrated DNA Technologies. An additional PARP13L-specific DsiRNA (sense: rGrGrArArUrCrUrArUrCrUrGrUrUr-CrGrArArUrArArUrUTT; antisense: rArArArArUrUrArUrUrC rGrArArCrArGrArUrArGrArUrUrCrCrArC) as described in (46) was obtained from Integrated DNA Technologies. A SMARTPool of four individual siRNAs against PARP12 was obtained from Horizon Discovery (M-013740-01-0005). When cells were approximately

50% confluent, 80 pmol of gene-specific DsiRNA or negative control nontargeting DsiRNA (Integrated DNA Technologies, 51-01-14-04) was added along with 4 μl of Lipofectamine 2000 (Invitrogen) to each well. These plates were incubated overnight, and then the wells of the same treatment were pooled before being split into 24-well plates, where the final infection experiments would take place. Information on biological replicates is indicated in each figure legend.

Quantification of knockdown was performed by reverse transcription quantitative PCR (RT-qPCR) following siRNA treatment as described above. Each siRNA treatment condition was performed in biological triplicate under conditions containing the final concentration of IFN-γ (100 U/ml). Cells were centrifuged at 500g for 1 min to pellet cells. Total RNA was then extracted using the Monarch Total RNA Miniprep Kit (New England BioLabs) according to the kit protocol. RNA concentrations and purity were measured using the NanoDrop Lite spectrophotometer (Thermo Fisher Scientific). For cDNA synthesis, 2 μg of total RNA was reverse transcribed using the High Capacity cDNA Reverse Transcription Kit (Thermo Fisher Scientific) in a final reaction volume of 20 μl. Quantitative PCR, measured in technical quadruplicate, was performed in a 96-well plate using the StepOnePlus Real-Time PCR System (Bio-Rad) and the Luna Universal qPCR Master Mix (New England BioLabs). Each reaction contained 10 μl of 1× qPCR Master Mix, 0.5 μM each of forward and reverse primers (see table S1), 2 μl of template DNA, and nuclease-free water (Thermo Fisher Scientific) to a final volume of 20 μl. Cycling protocol conditions were as follows: initial denaturation at 95°C for 60 s, followed by 40 cycles of denaturation at 95°C for 15 s and extension at 60°C for 30 s. Relative gene expression was quantified using the comparative C_T ($\Delta\Delta C_T$) method with GAPDH as the internal control. Results are presented as the fold change relative to a nontargeting siRNA treatment control.

Evolutionary and structural analyses of alphavirus macrodomains

All sequences used in viral macrodomain evolutionary analyses, listed by accession number and viral species, are shown in data S1 (tab 1). All nonredundant SFV nsP1 to nsP3 or nsP1 to nsP4 sequences (20 total), as well as additional polyprotein sequences from other viruses shown in data S1 (tab 1), were downloaded from the National Center for Biotechnology Information nonredundant database. Sequences were aligned in Geneious Prime 2022.1.1 (www.geneious.com/) software using Clustal Omega (72). The region corresponding to the SFV4 macrodomain (residues 1337 to 1496 from protein accession AKC01667.1) was extracted and realigned using Clustal Omega with two rounds of iterative refinement. The SFV consensus sequence shown in Fig. 2A was generated using Geneious software.

Structural models for the SFV4 macrodomain and SFV4 macrodomain with E48A substitution (representative of all other SFV isolates) were predicted using AlphaFold2 via the ColabFold package (41). The resulting structural models were compared to the experimentally determined model of the Getah virus macrodomain solved in complex with ADPr [Protein Data Bank code: 6R0G; (40)] using PyMOL (The PyMOL Molecular Graphics System, version 2.1, Schrödinger, LLC.).

Presence of PAR-binding-PARP domain architecture in metazoans

Sequences for human PARP7 (accession NP_001171646.1), PARP12 (accession NP_073587.1), and PARP13 (accession NP_064504.2)

were aligned using Clustal Omega with two rounds of iterative refinement. Sliding window sequence identity shown in Fig. 7A was generated in Geneious using a five-residue sliding window.

On the basis of the conservation of the PAR-binding domain (zinc-finger domain followed by two WWE domains) and PARP domain across all three human PARPs, we comprehensively searched for this domain architecture in two ways. First, we searched InterPro (www.ebi.ac.uk/interpro/search/ida/) (73) using the "Search By Domain Architecture" feature. Searching for proteins with a domain combination of a CCCH-type zinc-finger domain (InterPro entry: IPR000571) and then one or more WWE domains (InterPro entry: IPR004170), followed by a PARP domain (InterPro entry: IPR012317), yielded 349 proteins, all of which were from the metazoan clades shown in Fig. 7D (Cnidaria, Spiralia, Crustacea, and Deuterostoma).

To identify proteins that may not be represented in InterPro, we also performed iterative PSI-BLAST (74) searches as follows. The PAR-binding-PARP region of the human PARP12 (residues 270 to 698 of accession NP_073587.1) was used as a search query for the RefSeq database using PSI-BLAST with a e-value cutoff of 1×10^{-5}. To only capture proteins with PAR-binding-PARP architectures, only sequences with a sequence coverage cutoff of 90% or higher were retained for the next round. After two additional rounds of PSI-BLAST searching, the resulting 3159 sequences were analyzed by the organism clade. All sequences corresponded to the clades shown in Fig. 7D (Cnidaria, Spiralia, Crustacea, and Deuterostoma).

Phylogenetic analyses of PAR-binding-PARP domain–containing proteins

To generate a phylogeny of metazoan PAR-binding-PARP containing proteins, we downloaded full-length sequences for the 3159 proteins identified from our PSI-BLAST searches described above. Sequences were aligned using Clustal Omega (no iterative refinement), and incomplete and poorly aligning sequences were removed. To eliminate closely related sequences and reduce the total sequence number, sequences with >80% identity were reduced to a single unique sequence using CD-HIT with a 0.80 sequence identity cutoff (75), and human PARP7, PARP12, and PARP13 were added back in. The resulting 790 sequences are listed in data S1 (tab 2), including the accession number, species name, and GenBank annotation. All 790 full-length sequences were aligned using Clustal Omega with two rounds of iterative refinement, and maximum likelihood phylogenetic trees were generated using IQ-TREE (76). IQ-TREE phylogenies were generated using the "-bb 1000 -alrt 1000" commands for generation of 1000 ultrafast bootstrap (77) and SH-aLRT support values. The best-fitting substitution model was determined by ModelFinder (78) using the "-m AUTO" command. The resulting consensus phylogenetic tree was visualized using FigTree (http://tree.bio.ed.ac.uk/software/figtree/). Complete IQ-TREE–generated phylogenetic tree output, including bootstrap branch support, is shown in data S2. A second IQ-TREE phylogeny was generated using just the PAR-binding-PARP region of the protein alignment, corresponding to residues 270 to 698 of PARP12. That phylogenetic tree, which shows the same overall topology as the tree shown in Fig. 7E, is included in data S2.

Statistical analyses

Information on biological replicates is indicated in each figure legend. Statistical analyses on viral replication and RT-qPCR were performed using GraphPad Prism 9 (version 9.5.1). All experiments

were performed at least in triplicate ($N \geq 3$; exact values indicated in figure legends), with all data points displayed along with the means ± SD. Data were analyzed with the two-way analysis of variance (ANOVA) using Šidák's multiple comparison analysis. Asterisks (*) are used to indicate statistical significance [*$P < 0.05$; **$P < 0.01$; ***$P < 0.001$; ****$P < 0.0001$; n.s., not significant ($P > 0.05$)]. Maximum likelihood phylogenetic analyses were performed using IQ-TREE, using 1000 ultrafast bootstraps for branch support.

Supplementary Materials

The PDF file includes:
Figs. S1 to S8
Table S1
Legends for data S1 and S2

Other Supplementary Material for this manuscript includes the following:
Data S1 and S2

REFERENCES AND NOTES

1. J. G. M. Rack, L. Palazzo, I. Ahel, (ADP-ribosyl)hydrolases: Structure, function, and biology. *Genes Dev.* **34**, 263–284 (2020).
2. N. C. Hoch, L. M. Polo, ADP-ribosylation: From molecular mechanisms to human disease. *Genet. Mol. Biol.* **43**, e20190075 (2020).
3. M. S. Cohen, P. Chang, Insights into the biogenesis, function, and regulation of ADP-ribosylation. *Nat. Chem. Biol.* **14**, 236–243 (2018).
4. B. Luscher, I. Ahel, M. Altmeyer, A. Ashworth, P. Bai, P. Chang, M. Cohen, D. Corda, F. Dantzer, M. D. Daugherty, T. M. Dawson, V. L. Dawson, S. Deindl, A. R. Fehr, K. L. H. Feijs, D. V. Filippov, J. P. Gagne, G. Grimaldi, S. Guettler, N. C. Hoch, M. O. Hottiger, P. Korn, W. L. Kraus, A. Ladurner, L. Lehtio, A. K. L. Leung, C. J. Lord, A. Mangerich, I. Matic, J. Matthews, G. L. Moldovan, J. Moss, G. Natoli, M. L. Nielsen, M. Niepel, J. Pascal, B. M. Paschal, K. Pawlowski, G. G. Poirier, S. Smith, G. Timinszky, Z.-Q. Wang, J. Yelamos, X. Yu, R. Zaja, M. Ziegler, ADP-ribosyltransferases, an update on function and nomenclature. *FEBS J.* **289**, 7399–7410 (2022).
5. B. Luscher, M. Butepage, L. Eckei, S. Krieg, P. Verheugd, B. H. Shilton, ADP-ribosylation, a multifaceted posttranslational modification involved in the control of cell physiology in health and disease. *Chem. Rev.* **118**, 1092–1136 (2018).
6. K. L. H. Feijs, A. H. Forst, P. Verheugd, B. Luscher, Macrodomain-containing proteins: Regulating new intracellular functions of mono(ADP-ribosyl)ation. *Nat. Rev. Mol. Cell Biol.* **14**, 443–451 (2013).
7. R. Gupte, Z. Liu, W. L. Kraus, PARPs and ADP-ribosylation: Recent advances linking molecular functions to biological outcomes. *Genes Dev.* **31**, 101–126 (2017).
8. A. R. Fehr, S. A. Singh, C. M. Kerr, S. Mukai, H. Higashi, M. Aikawa, The impact of PARPs and ADP-ribosylation on inflammation and host-pathogen interactions. *Genes Dev.* **34**, 341–359 (2020).
9. L. M. Iyer, A. M. Burroughs, V. Anantharaman, L. Aravind, Apprehending the NAD⁺-ADPr-dependent systems in the virus world. *Viruses* **14**, 1977 (2022).
10. B. Luscher, M. Verheirstraeten, S. Krieg, P. Korn, Intracellular mono-ADP-ribosyltransferases at the host-virus interphase. *Cell. Mol. Life Sci.* **79**, 288 (2022).
11. H. Zhu, C. Zheng, When PARPs meet antiviral innate immunity. *Trends Microbiol.* **29**, 776–778 (2021).
12. Q. Du, Y. Miao, W. He, H. Zheng, ADP-ribosylation in antiviral innate immune response. *Pathogens* **12**, 303 (2023).
13. J. W. Schoggins, C. M. Rice, Interferon-stimulated genes and their antiviral effector functions. *Curr. Opin. Virol.* **1**, 519–525 (2011).
14. S. Atasheva, M. Akhrymuk, E. I. Frolova, I. Frolov, New PARP gene with an anti-alphavirus function. *J. Virol.* **86**, 8147–8160 (2012).
15. M. D. Daugherty, J. M. Young, J. A. Kerns, H. S. Malik, Rapid evolution of PARP genes suggests a broad role for ADP-ribosylation in host-virus conflicts. *PLOS Genet.* **10**, e1004403 (2014).
16. J. A. Kerns, M. Emerman, H. S. Malik, Positive selection and increased antiviral activity associated with the PARP-containing isoform of human zinc-finger antiviral protein. *PLOS Genet.* **4**, e21 (2008).
17. A. K. L. Leung, D. E. Griffin, J. Bosch, A. R. Fehr, The conserved macrodomain is a potential therapeutic target for coronaviruses and alphaviruses. *Pathogens* **11**, 94 (2022).
18. J. G. M. Rack, V. Zorzini, Z. Zhu, M. Schuller, D. Ahel, I. Ahel, Viral macrodomains: A structural and evolutionary assessment of the pharmacological potential. *Open Biol.* **10**, 200237 (2020).
19. A. R. Fehr, R. Channappanavar, G. Jankevicius, C. Fett, J. Zhao, J. Athmer, D. K. Meyerholz, I. Ahel, S. Perlman, The conserved coronavirus macrodomain promotes virulence and suppresses the innate immune response during severe acute respiratory syndrome coronavirus infection. *MBio* **7**, e0172116 (2016).
20. T. Kuri, K. K. Eriksson, A. Putics, R. Zust, E. J. Snijder, A. D. Davidson, S. G. Siddell, V. Thiel, J. Ziebuhr, F. Weber, The ADP-ribose-1-monophosphatase domains of severe acute respiratory syndrome coronavirus and human coronavirus 229E mediate resistance to antiviral interferon responses. *J. Gen. Virol.* **92**, 1899–1905 (2011).
21. R. Abraham, D. Hauer, R. L. McPherson, A. Utt, I. T. Kirby, M. S. Cohen, A. Merits, A. K. L. Leung, D. E. Griffin, ADP-ribosyl-binding and hydrolase activities of the alphavirus nsP3 macrodomain are critical for initiation of virus replication. *Proc. Natl. Acad. Sci. U.S.A.* **115**, E10457–E10466 (2018).
22. R. L. McPherson, R. Abraham, E. Sreekumar, S.-E. Ong, S.-J. Cheng, V. K. Baxter, H. A. Kistemaker, D. V. Filippov, D. E. Griffin, A. K. L. Leung, ADP-ribosylhydrolase activity of Chikungunya virus macrodomain is critical for virus replication and virulence. *Proc. Natl. Acad. Sci. U.S.A.* **114**, 1666–1671 (2017).
23. E. Park, D. E. Griffin, The nsP3 macro domain is important for Sindbis virus replication in neurons and neurovirulence in mice. *Virology* **388**, 305–314 (2009).
24. E. G. Aguilar, G. Paniccia, C. Adura, Z. S. Singer, A. W. Ashbrook, B. S. Razooky, C. M. Rice, M. R. MacDonald, Sindbis macrodomain poly-ADP-ribose hydrolase activity is important for viral RNA synthesis. *J. Virol.* **96**, e0151621 (2022).
25. M. E. Grunewald, Y. Chen, C. Kuny, T. Maejima, R. Lease, D. Ferraris, M. Aikawa, C. S. Sullivan, S. Perlman, A. R. Fehr, The coronavirus macrodomain is required to prevent PARP-mediated inhibition of virus replication and enhancement of IFN expression. *PLOS Pathog.* **15**, e1007756 (2019).
26. C. M. Kerr, S. Parthasarathy, N. Schwarting, J. J. O'Connor, J. J. Pfannenstiel, E. Giri, S. More, R. C. Orozco, A. R. Fehr, PARP12 is required to repress the replication of a Mac1 mutant coronavirus in a cell- and tissue-specific manner. *J. Virol.* **97**, e0088523 (2023).
27. H. Otto, P. A. Reche, F. Bazan, K. Dittmar, F. Haag, F. Koch-Nolte, In silico characterization of the family of PARP-like poly(ADP-ribosyl)transferases (pARTs). *BMC Genomics* **6**, 139 (2005).
28. C.-S. Yang, K. Jividen, A. Spencer, N. Dworak, L. Ni, L. T. Oostdyk, M. Chatterjee, B. Kusmider, B. Reon, M. Parlak, V. Gorbunova, T. Abbas, E. Jeffery, N. E. Sherman, B. M. Paschal, Ubiquitin modification by the E3 ligase/ADP-ribosyltransferase Dtx3L/Parp9. *Mol. Cell* **66**, 503–516.e5 (2017).
29. M. J. Bick, J.-W. N. Carroll, G. Gao, S. P. Goff, C. M. Rice, M. R. MacDonald, Expression of the zinc-finger antiviral protein inhibits alphavirus replication. *J. Virol.* **77**, 11555–11562 (2003).
30. H. Iwata, C. Goettsch, A. Sharma, P. Ricchiuto, W. W. B. Goh, A. Halu, I. Yamada, H. Yoshida, T. Hara, M. Wei, N. Inoue, D. Fukuda, A. Mojcher, P. C. Mattson, A. L. Barabasi, M. Boothby, E. Aikawa, S. A. Singh, M. Aikawa, PARP9 and PARP14 cross-regulate macrophage activation via STAT1 ADP-ribosylation. *Nat. Commun.* **7**, 12849 (2016).
31. Y. Zhang, D. Mao, W. T. Roswit, X. Jin, A. C. Patel, D. A. Patel, E. Agapov, Z. Wang, R. M. Tidwell, J. J. Atkinson, G. Huang, R. McCarthy, J. Yu, N. E. Yun, S. Paessler, T. G. Lawson, N. S. Omattage, T. J. Brett, M. J. Holtzman, PARP9-DTX3L ubiquitin ligase targets host histone H2BJ and viral 3C protease to enhance interferon signaling and control viral infection. *Nat. Immunol.* **16**, 1215–1227 (2015).
32. A. Z. Lu, R. Abo, Y. Ren, B. Gui, J.-R. Mo, D. Blackwell, T. Wigle, H. Keilhack, M. Niepel, Enabling drug discovery for the PARP protein family through the detection of mono-ADP-ribosylation. *Biochem. Pharmacol.* **167**, 97–106 (2019).
33. S. Vyas, I. Matic, L. Uchima, J. Rood, R. Zaja, R. T. Hay, I. Ahel, P. Chang, Family-wide analysis of poly(ADP-ribose) polymerase activity. *Nat. Commun.* **5**, 4426 (2014).
34. N. Garmashova, R. Gorchakov, E. Frolova, I. Frolov, Sindbis virus nonstructural protein nsP2 is cytotoxic and inhibits cellular transcription. *J. Virol.* **80**, 5686–5696 (2006).
35. C. Li, Y. Debing, G. Jankevicius, I. Ahel, B. Coutard, B. Canard, Viral macro domains reverse protein ADP-ribosylation. *J. Virol.* **90**, 8478–8486 (2016).
36. S. E. Delgado-Rodriguez, A. P. Ryan, M. D. Daugherty, Recurrent loss of macrodomain activity in host immunity and viral proteins. *Pathogens* **12**, 674 (2023).
37. P. Berglund, M. Sjoberg, H. Garoff, G. J. Atkins, B. J. Sheahan, P. Liljestrom, Semliki Forest virus expression system: Production of conditionally infectious recombinant particles. *Biotechnology* **11**, 916–920 (1993).
38. P. Liljestrom, H. Garoff, Expression of proteins using Semliki Forest virus vectors. *Curr. Protoc. Mol. Biol.* 10.1002/0471142727.mb1620s29 , (2001).
39. F. Nasar, G. Palacios, R. V. Gorchakov, H. Guzman, A. P. Da Rosa, N. Savji, V. L. Popov, M. B. Sherman, W. I. Lipkin, R. B. Tesh, S. C. Weaver, Eilat virus, a unique alphavirus with host range restricted to insects by RNA replication. *Proc. Natl. Acad. Sci. U.S.A.* **109**, 14622–14627 (2012).
40. A. S. Ferreira-Ramos, G. Sulzenbacher, B. Canard, B. Coutard, Snapshots of ADP-ribose bound to Getah virus macro domain reveal an intriguing choreography. *Sci. Rep.* **10**, 14422 (2020).
41. M. Mirdita, K. Schutze, Y. Moriwaki, L. Heo, S. Ovchinnikov, M. Steinegger, ColabFold: Making protein folding accessible to all. *Nat. Methods* **19**, 679–682 (2022).

42. F. Rosenthal, K. L. Feijs, E. Frugier, M. Bonalli, A. H. Forst, R. Imhof, H. C. Winkler, D. Fischer, A. Caflisch, P. O. Hassa, B. Luscher, M. O. Hottiger, Macrodomain-containing proteins are new mono-ADP-ribosylhydrolases. *Nat. Struct. Mol. Biol.* **20**, 502–507 (2013).

43. G. Jankevicius, M. Hassler, B. Golia, V. Rybin, M. Zacharias, G. Timinszky, A. G. Ladurner, A family of macrodomain proteins reverses cellular mono-ADP-ribosylation. *Nat. Struct. Mol. Biol.* **20**, 508–514 (2013).

44. K. M. Rodriguez, S. C. Buch-Larsen, I. T. Kirby, I. R. Siordia, D. Hutin, M. Rasmussen, D. M. Grant, L. L. David, J. Matthews, M. L. Nielsen, M. S. Cohen, Chemical genetics and proteome-wide site mapping reveal cysteine MARylation by PARP-7 on immune-relevant protein targets. *eLife* **10**, e60480 (2021).

45. D. P. DiCiommo, R. Bremner, Rapid, high level protein production using DNA-based Semliki Forest virus vectors. *J. Biol. Chem.* **273**, 18060–18066 (1998).

46. J. Schwerk, F. W. Soveg, A. P. Ryan, K. R. Thomas, L. D. Hatfield, S. Ozarkar, A. Forero, A. M. Kell, J. A. Roby, L. So, J. L. Hyde, M. Gale Jr., M. D. Daugherty, R. Savan, RNA-binding protein isoforms ZAP-S and ZAP-L have distinct antiviral and immune resolution functions. *Nat. Immunol.* **20**, 1610–1620 (2019).

47. M. M. H. Li, E. G. Aguilar, E. Michailidis, J. Pabon, P. Park, X. Wu, Y. P. de Jong, W. M. Schneider, H. Molina, C. M. Rice, M. R. MacDonald, Characterization of novel splice variants of zinc finger antiviral protein (ZAP). *J. Virol.* **93**, e00715–e00719 (2019).

48. G. Charron, M. M. Li, M. R. MacDonald, H. C. Hang, Prenylome profiling reveals S-farnesylation is crucial for membrane targeting and antiviral activity of ZAP long-isoform. *Proc. Natl. Acad. Sci. U.S.A.* **110**, 11085–11090 (2013).

49. M. M. Li, Z. Lau, P. Cheung, E. G. Aguilar, W. M. Schneider, L. Bozzacco, H. Molina, E. Buehler, A. Takaoka, C. M. Rice, D. P. Felsenfeld, M. R. MacDonald, TRIM25 enhances the antiviral action of zinc-finger antiviral protein (ZAP). *PLOS Pathog.* **13**, e1006145 (2017).

50. R. Abraham, R. L. McPherson, M. Dasovich, M. Badiee, A. K. L. Leung, D. E. Griffin, Both ADP-ribosyl-binding and hydrolase activities of the alphavirus nsP3 macrodomain affect neurovirulence in mice. *MBio* **11**, 11:10.1128/mbio.03253-19 (2020).

51. E. I. Frolova, O. Palchevska, F. Dominguez, I. Frolov, Alphavirus-induced transcriptional and translational shutoffs play major roles in blocking the formation of stress granules. *J. Virol.* **97**, e0097923 (2023).

52. E. Park, D. E. Griffin, Interaction of Sindbis virus non-structural protein 3 with poly(ADP-ribose) polymerase 1 in neuronal cells. *J. Gen. Virol.* **90**, 2073–2080 (2009).

53. S. Karki, M. M. Li, J. W. Schoggins, S. Tian, C. M. Rice, M. R. MacDonald, Multiple interferon stimulated genes synergize with the zinc finger antiviral protein to mediate anti-alphavirus activity. *PLOS ONE* **7**, e37398 (2012).

54. R. Burdeinick-Kerr, D. Govindarajan, D. E. Griffin, Noncytolytic clearance of sindbis virus infection from neurons by gamma interferon is dependent on Jak/STAT signaling. *J. Virol.* **83**, 3429–3435 (2009).

55. R. Burdeinick-Kerr, D. E. Griffin, Gamma interferon-dependent, noncytolytic clearance of sindbis virus infection from neurons in vitro. *J. Virol.* **79**, 5374–5385 (2005).

56. L. C. Russo, R. Tomasin, I. A. Matos, A. C. Manucci, S. T. Sowa, K. Dale, K. W. Caldecott, L. Lehtio, D. Schechtman, F. C. Meotti, A. Bruni-Cardoso, N. C. Hoch, The SARS-CoV-2 Nsp3 macrodomain reverses PARP9/DTX3L-dependent ADP-ribosylation induced by interferon signaling. *J. Biol. Chem.* **297**, 101041 (2021).

57. P. Kar, C. Chatrin, N. Dukic, O. Suyari, M. Schuller, K. Zhu, E. Prokhorova, N. Bigot, D. Baretic, J. Ahel, J. D. Elsborg, M. L. Nielsen, T. Clausen, S. Huet, M. Niepel, S. Sanyal, D. Ahel, R. Smith, I. Ahel, PARP14 and PARP9/DTX3L regulate interferon-induced ADP-ribosylation. *EMBO J.* **43**, 2929–2953 (2024).

58. V. C. Ribeiro, L. C. Russo, N. C. Hoch, PARP14 is regulated by the PARP9/DTX3L complex and promotes interferon gamma-induced ADP-ribosylation. *EMBO J.* **43**, 2908–2928 (2024).

59. C. C. Gunderson, K. N. Moore, Olaparib: An oral PARP-1 and PARP-2 inhibitor with promising activity in ovarian cancer. *Future Oncol.* **11**, 747–757 (2015).

60. G. Xue, M. Braczyk, D. Goncalves-Carneiro, D. M. Dawidziak, K. Sanchez, H. Ong, Y. Wan, K. K. Zadrozny, B. K. Ganser-Pornillos, P. D. Bieniasz, O. Pornillos, Poly(ADP-ribose) potentiates ZAP antiviral activity. *PLOS Pathog.* **18**, e1009202 (2022).

61. S. R. Margolis, P. A. Dietzen, B. M. Hayes, S. C. Wilson, B. C. Remick, S. Chou, R. E. Vance, The cyclic dinucleotide 2′3′-cGAMP induces a broad antibacterial and antiviral response in the sea anemone Nematostella vectensis. *Proc. Natl. Acad. Sci. U.S.A.* **118**, e2109022118 (2021).

62. P. Liljestrom, H. Garoff, A new generation of animal cell expression vectors based on the Semliki Forest virus replicon. *Biotechnology* **9**, 1356–1361 (1991).

63. B. J. Kelly, M. N. Fleeton, G. J. Atkins, Potential of alphavirus vectors in the treatment of advanced solid tumors. *Recent Pat. Anticancer Drug Discov.* **2**, 159–166 (2007).

64. K. Lundstrom, Alphavirus-based vaccines. *Viruses* **6**, 2392–2415 (2014).

65. A. Zajakina, K. Spunde, K. Lundstrom, Application of alphaviral vectors for immunomodulation in cancer therapy. *Curr. Pharm. Des.* **23**, 4906–4932 (2017).

66. A. Singh, G. Koutsoumpli, S. van de Wall, T. Daemen, An alphavirus-based therapeutic cancer vaccine: From design to clinical trial. *Cancer Immunol. Immunother.* **68**, 849–859 (2019).

67. Y. M. Alhammad, S. Parthasarathy, R. Ghimire, C. M. Kerr, J. J. O'Connor, J. J. Pfannenstiel, D. Chanda, A. M. Miller, N. Baumlin, M. Salathe, R. L. Unckless, S. Zuniga, L. Enjuanes, S. More, R. Channappanavar, A. R. Fehr, SARS-CoV-2 Mac1 is required for IFN antagonism and efficient virus replication in cell culture and in mice. *Proc. Natl. Acad. Sci. U.S.A.* **120**, e2302083120 (2023).

68. D. Goncalves-Carneiro, M. A. Takata, H. Ong, A. Shilton, P. D. Bieniasz, Origin and evolution of the zinc finger antiviral protein. *PLOS Pathog.* **17**, e1009545 (2021).

69. M. D. Daugherty, H. S. Malik, Rules of engagement: Molecular insights from host-virus arms races. *Annu. Rev. Genet.* **46**, 677–700 (2012).

70. C. K. Donawho, Y. Luo, Y. Luo, T. D. Penning, J. L. Bauch, J. J. Bouska, V. D. Bontcheva-Diaz, B. F. Cox, T. L. DeWeese, L. E. Dillehay, D. C. Ferguson, N. S. Ghoreishi-Haack, D. R. Grimm, R. Guan, E. K. Han, R. R. Holley-Shanks, B. Hristov, K. B. Idler, K. Jarvis, E. F. Johnson, L. R. Kleinberg, V. Klinghofer, L. M. Lasko, X. Liu, K. C. Marsh, T. P. McGonigal, J. A. Meulbroek, A. M. Olson, J. P. Palma, L. E. Rodriguez, Y. Shi, J. A. Stavropoulos, A. C. Tsurutani, G. D. Zhu, S. H. Rosenberg, V. L. Giranda, D. J. Frost, ABT-888, an orally active poly(ADP-ribose) polymerase inhibitor that potentiates DNA-damaging agents in preclinical tumor models. *Clin. Cancer Res.* **13**, 2728–2737 (2007).

71. A. G. Thorsell, T. Ekblad, T. Karlberg, M. Low, A. F. Pinto, L. Tresaugues, M. Moche, M. S. Cohen, H. Schuler, Structural basis for potency and promiscuity in poly(ADP-ribose) polymerase (PARP) and tankyrase inhibitors. *J. Med. Chem.* **60**, 1262–1271 (2017).

72. F. Sievers, A. Wilm, D. Dineen, T. J. Gibson, K. Karplus, W. Li, R. Lopez, H. McWilliam, M. Remmert, J. Söding, J. D. Thompson, D. G. Higgins, Fast, scalable generation of high-quality protein multiple sequence alignments using Clustal Omega. *Mol. Syst. Biol.* **7**, 539 (2011).

73. T. Paysan-Lafosse, M. Blum, S. Chuguransky, T. Grego, B. L. Pinto, G. A. Salazar, M. L. Bileschi, P. Bork, A. Bridge, L. Colwell, J. Gough, D. H. Haft, I. Letunic, A. Marchler-Bauer, H. Mi, D. A. Natale, C. A. Orengo, A. P. Pandurangan, C. Rivoire, C. J. A. Sigrist, I. Sillitoe, N. Thanki, P. D. Thomas, S. C. E. Tosatto, C. H. Wu, A. Bateman, InterPro in 2022. *Nucleic Acids Res.* **51**, D418–D427 (2023).

74. S. F. Altschul, T. L. Madden, A. A. Schäffer, J. Zhang, Z. Zhang, W. Miller, D. J. Lipman, Gapped BLAST and PSI-BLAST: A new generation of protein database search programs. *Nucleic Acids Res.* **25**, 3389–3402 (1997).

75. W. Li, A. Godzik, Cd-hit: A fast program for clustering and comparing large sets of protein or nucleotide sequences. *Bioinformatics* **22**, 1658–1659 (2006).

76. L.-T. Nguyen, H. A. Schmidt, A. von Haeseler, B. Q. Minh, IQ-TREE: A fast and effective stochastic algorithm for estimating maximum-likelihood phylogenies. *Mol. Biol. Evol.* **32**, 268–274 (2015).

77. D. T. Hoang, O. Chernomor, A. von Haeseler, B. Q. Minh, L. S. Vinh, UFBoot2: Improving the ultrafast bootstrap approximation. *Mol. Biol. Evol.* **35**, 518–522 (2018).

78. S. Kalyaanamoorthy, B. Q. Minh, T. K. F. Wong, A. von Haeseler, L. S. Jermiin, ModelFinder: Fast model selection for accurate phylogenetic estimates. *Nat. Methods* **14**, 587–589 (2017).